

AD-A279 446



AL/CF-SR-1994-0002



**ADVANCED FILTERING METHODS IN HEAD
TELEOPERATED SYSTEMS AND
HELMET MOUNTED DISPLAYS (U)**

DTIC
ELECTE
MAY 19 1994
S-B D

**S.J. Merhav
S. Lifshitz**

**TECHNION-ISRAEL INSTITUTE OF TECHNOLOGY
TECHNION R&D FOUNDATION LTD.
TECHNION CITY, HAIFA 3200 ISRAEL**

Dean F. Kocian

**VISUAL DISPLAY SYSTEMS BRANCH
CREW SYSTEMS DIRECTORATE
HUMAN ENGINEERING DIVISION
WRIGHT-PATTERSON AFB OH 45433-7022**

September 1990

FINAL REPORT FOR PERIOD SEPTEMBER 1989 - AUGUST 1990

Approved for public release; distribution is unlimited

**AIR FORCE MATERIEL COMMAND
WRIGHT-PATTERSON AIR FORCE BASE, OHIO 45433**

94-15019

68P

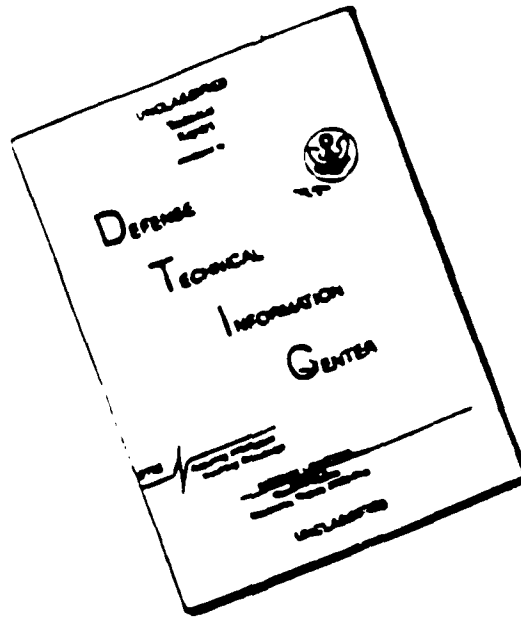
**A
R
M
S
T
R
O
N
G

L
A
B
O
R
A
T
O
R
Y**

94 5 18 117

UNCLASSIFIED

DISCLAIMER NOTICE



THIS DOCUMENT IS BEST
QUALITY AVAILABLE. THE COPY
FURNISHED TO DTIC CONTAINED
A SIGNIFICANT NUMBER OF
PAGES WHICH DO NOT
REPRODUCE LEGIBLY.

NOTICES

When US Government drawings, specifications, or other data are used for any purpose other than a definitely related Government procurement operation, the Government thereby incurs no responsibility nor any obligation whatsoever, and the fact that the Government may have formulated, furnished, or in any way supplied the said drawings, specifications, or other data, is not to be regarded by implication or otherwise, as in any manner licensing the holder or any other person or corporation, or conveying any rights or permission to manufacture, use, or sell any patented invention that may in any way be related thereto.

Please do not request copies of this report from the Armstrong Laboratory. Additional copies may be purchased from:

National Technical Information Service
5285 Royal Road
Springfield, Virginia 22161

Federal Government agencies and their contractors registered with the Defense Technical Information Center should direct requests for copies of this report to:

Defense Technical Information Center
Cameron Station
Alexandria, Virginia 22314

DISCLAIMER

This Special Report is published as received
and has not been edited by the Technical Editing
Staff of the Armstrong Laboratory.

TECHNICAL REVIEW AND APPROVAL

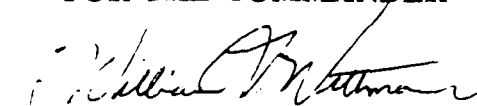
AL/CF-SR-1994-0002

This report has been reviewed by the Office of Public Affairs (PA) and is releasable to the National Technical Information Service (NTIS). At NTIS, it will be available to the general public, including foreign nations.

The voluntary informed consent of the subjects used in this research was obtained as required by Air Force Regulation 169-3.

This technical report has been reviewed and is approved for publication.

FOR THE COMMANDER


KENNETH R. BOFF, Chief
Human Engineering Division
Armstrong Laboratory

Accession For	
NTIS GPA&I	<input checked="checked" type="checkbox"/>
DTIC TAB	<input type="checkbox"/>
Unannounced	<input type="checkbox"/>
Justification	
By	
Distribution/	
Availability Codes	
Dist	Special
A	

REPORT DOCUMENTATION PAGE

FORM APPROVED
DMB No. 0704-0168

1. TITLE AND SUBTITLE
2. AUTHOR(s)
3. REPORT TYPE AND DATES COVERED
4. PERFORMING ORGANIZATION NAME(S) AND ADDRESS(ES)
5. FUNDING NUMBERS
6. PERFORMING ORGANIZATION REPORT NUMBER
7. SPONSORING / MONITORING AGENCY NAME(S) AND ADDRESS(ES)
8. SPONSORING / MONITORING AGENCY REPORT NUMBER
9. SUPPLEMENTARY NOTES
10. DISTRIBUTION / AVAILABILITY STATEMENT
11. DISTRIBUTION CODE
12. NUMBER OF PAGES
13. PRICE CODE
14. LIMITATION OF ABSTRACT

1. TITLE AND SUBTITLE
2. AUTHOR(s)
3. REPORT TYPE AND DATES COVERED
4. PERFORMING ORGANIZATION NAME(S) AND ADDRESS(ES)
5. FUNDING NUMBERS
6. PERFORMING ORGANIZATION REPORT NUMBER
7. SPONSORING / MONITORING AGENCY NAME(S) AND ADDRESS(ES)
8. SPONSORING / MONITORING AGENCY REPORT NUMBER
9. SUPPLEMENTARY NOTES
10. DISTRIBUTION / AVAILABILITY STATEMENT
11. DISTRIBUTION CODE
12. NUMBER OF PAGES
13. PRICE CODE
14. LIMITATION OF ABSTRACT

Advanced Filtering Methods in Head Teleoperated Systems and Helmet Mounted Displays

5. FUNDING NUMBERS
PR: 2313
TA: V2
WU: OB

*S. J. Merhav
*S. Lifshitz
Dean F. Kocian

REPORTING ORGANIZATION NAME(S) AND ADDRESS(ES)
* Technion-Israel Institute of Technology
c/o Technion R&D Foundation Ltd.
Technion City, Haifa 32000 Israel

6. PERFORMING ORGANIZATION
REPORT NUMBER

SPONSORING / MONITORING AGENCY NAME(S) AND ADDRESS(ES)
Armstrong Laboratory, Crew Systems Directorate
Human Engineering Division
Human Systems Center AFMC
Air Force Materiel Command
Wright-Patterson AFB OH 45433-7022

7. SPONSORING / MONITORING
AGENCY REPORT NUMBER
AL/CF-SR-1994-0002

9. SUPPLEMENTARY NOTES

10. DISTRIBUTION / AVAILABILITY STATEMENT

11. DISTRIBUTION CODE

Approved for public release; distribution is unlimited.

This paper address errors caused by vibration or turbulence in airborne helmet displays and teleoperation. It is shown by analysis and computer simulations that a modified version of the LMS adaptive noise suppression algorithm facilitates the separation of the large voluntary head movements from the vibration-induced small nonvoluntary head motion. Thus, the effects of the biodynamic interferences can be essentially removed. The results also indicate that errors in head tracking teleoperated devices can essentially be suppressed. Extensive man-in-the-loop laboratory simulations which validate the method are described.

12. NUMBER OF PAGES

69

Biodynamic interference, noise suppression, adaptive filtering, teleoperation, helmet mounted displays

13. PRICE CODE

14. LIMITATION OF ABSTRACT

Unclassified

Unclassified

Unclassified

Unlimited

LIST OF CONTENTS

	<u>Page</u>
Part 1:	
Adaptive Suppression of Biodynamic Interference In Helmet Mounted Displays and Head Teleoperation.	1
Abstract	1
Introduction	1
Stabilization of Helmet Displays	2
The Adaptive Filter	3
Computer Simulations	10
Experimental Validation	13
Conclusions	16
Acknowledgments	17
References	18
Figures	20
 Part 2:	
Man-In-The-Loop Study of Filtering For Airborne Head Tracking Tasks.	33
Abstract	33
Introduction	34
Principle of Operation	36
Experimental Investigation	37
Summary of Experimental Results	48
Acknowledgments	48
References	49
Appendix: The Adaptive Filter	51
Figures	55

ADAPTIVE SUPPRESSION OF BIODYNAMIC INTERFERENCE IN HELMET
MOUNTED DISPLAYS AND HEAD TELEOPERATION

S. Lifshitz[#] and S. J. Merhav^{*}

Department of Aerospace Engineering, Technion, Haifa - Israel

Abstract

This paper addresses errors caused by vibration or turbulence in airborne helmet displays and teleoperation. It is shown by analysis and computer simulations that a modified version of the LMS adaptive noise suppression algorithm facilitates the separation of the large voluntary head movements from the vibration-induced small nonvoluntary head motion. Thus, the effects of the biodynamic interference can be essentially removed. The results also indicate that errors in head tracking teleoperated devices can essentially be suppressed. Extensive man-in-the-loop laboratory simulations which validate the method are described.

1. Introduction

System teleoperation by pilot head motion and presentation of computer generated symbols and flight information in helmet mounted displays is emerging as a promising technology in modern avionic systems. Head teleoperation is potentially an effective method for instinctive and rapid aiming of radar antennas, missile seeker heads or laser designators. In addition, it relieves the hands of the pilot for other vital manual tasks in increasingly complex airborne

This paper is based on the M.Sc. thesis of the first author

[#] Graduate student

^{*} Professor, Head Flight Control Laboratory

environments. Helmet mounted displays (HMD) can, in principle, be the ultimate solution in merging computer generated displays with the outside scene, thus embracing the entire field of view available to the pilot. Therefore, the HMD potentially relieves the pilot from the troublesome need to share his attention between the all-aspect outside scene and a restrictive cockpit mounted panel or head-up display.

However, a potential shortcoming of head teleoperation and HMD's is their vulnerability to biodynamic interference resulting from vibration, atmospheric turbulence or self-induced vehicle motion. These interferences can cause substantial random aiming errors and apparent display blurring which may seriously impair pilot performance. Two kinds of biodynamic interference exist, namely: 1. Additive interferences due to nonvoluntary limb motions caused by, and correlated with, vibration, Levison et al.¹, Jex². 2. Nonadditive interferences resulting from the disturbances in the central nervous system caused by the body and head vibrations, uncorrelated with them, but monotonically increasing with their intensity, Wells and Griffin^{3,4}. Head vibration causes relative angular motion of the HMD with respect to the line of sight of the eye which is inertially stabilized by the vestibular system. Consequently, as a result of the apparent display shift, image blurring occurs, resulting in substantial degradation of reading speed and probability of correct character recognition, Lewis and Griffin⁵ and Wells and Griffin⁶. This neuromotor stabilization, known as the Vestibulo-Ocular Reflex (VOR) is effective in the frequency range of 2 to 10 Hz, Benson and Barnes⁷. Wells and Griffin^{6,8} conducted experiments to cancel this blurring by shifting the display in the opposite direction with an amplitude equal to the measured head motion which was determined by an approximate double integration of head angular acceleration. They succeeded in demonstrating the effectiveness of the concept, but, the imperfection of the integration caused substantial transients in the display position in the presence of large angular

head motion.

In this paper a method for display stabilization, based on a modified Adaptive Noise Cancellation (ANC), Merhav⁹, is described. It is designed to fulfill the following requirements:

1. Suppression of the additive nonvoluntary head motion due to vibration even in the presence of large voluntary head motion.
2. Rapid adaptation to changing parameters in the biodynamic model of the pilot due to changes in posture and muscle tone.

Extensive computer simulations with a linear biodynamic model were performed. These demonstrated the effectiveness of the Adaptive Filter (AF) in suppressing the effects of additive biodynamic interference. Subsequently, extensive man-in-the-loop experiments were conducted on a six degrees-of-freedom simulator which was driven by vertical vibration commands representing typical helicopter vibration spectra. The results of these tests proved to have excellent correspondence with the computer simulations and they demonstrated their effectiveness under essentially realistic flight conditions.

2. Stabilization of Helmet Displays

The principle of operation of helmet display stabilization is described with the aid of Fig.1. The aircraft A/C is viewed through the transparent helmet visor. The hexagon S represents a reticle symbol element generated in the helmet mounted CRT and is projected to optical infinity. Platform accelerations, a , excite the biodynamic angular head motion, α , which is detected by the six degrees-of-freedom head motion sensor, P, providing the voluntary head motion signal, U_c , along with the signal U_b which represents the additive nonvoluntary head motion. α causes S to move with respect to the line of sight to A/C which remains fixed on the retina because of the vestibulo-ocular reflex. The search and track voluntary head motion, also detected by P, is denoted by U_c . The

total head motion signal, $U_t = U_c + U_b$, would normally drive the teleoperated device inducing aiming errors due to U_b . The block Y_b , shown in dotted lines, represents the biodynamic model which can be representative of different limbs or body elements. The relative angular deviation, α , between the stabilized line of sight and the reticle, S , can cause apparent display blurring indicated by S' . The display stabilization signals are provided by the adaptive filter as follows: Platform mounted inertial sensors consisting of accelerometers or gyroscopes, sense the signal a' which is linearly correlated with a and the angular head motion α . The output \hat{U}_b of AF is compared to $U_t = U_c + U_b$. The error e drives the adaptive algorithm in AF so that its internal parameters automatically adjust to minimize e^2 . It is easily seen that this occurs when $U_b - \hat{U}_b \stackrel{\Delta}{=} \bar{U}_b \rightarrow 0$. This method, known as adaptive noise canceling (ANC), Widrow and McCool⁹, considerably reduces the biodynamic interference component U_b without essentially affecting U_c . In order to stabilize computer generated symbols such as S , \hat{U}_b is fed into the display generator, so that S is shifted by $\alpha_s = -\alpha$, which is thus stabilized with respect to the line of sight and consequently, display blurring is essentially suppressed. The estimated voluntary head motion $U_f \stackrel{\Delta}{=} U_t - \hat{U}_b$ is the signal used to drive the teleoperated device. The algorithm, described here in the elevation axis only, must, in principle, be implemented in azimuth as well. However, since vibration is primarily along the vertical, the biodynamic interference in azimuth is marginal as compared to elevation. For this reason, and practical considerations, the adaptive filter was implemented in elevation only in the experiments described in this paper.

3. The Adaptive Filter

The adaptive filter is based on the well known LMS algorithm widely used in adaptive noise cancellation applications. It is an extension of the classical LMS described in Widrow and McCool¹⁰. Its main advantages are small computational

load, global stability and robustness. The extended LMS presented in this paper has the additional advantages of rapid adaptation to variations in model parameters and the precise estimation of the relatively small disturbance U_b in the presence of large voluntary head motion U_c . This issue is addressed in Merhav⁹. Other algorithms such as RLS and Lattice filters, Haykin¹¹, Honig and Messerschmitt¹², were considered because of their superior convergence in terms of the number of iterations. However, in view of their larger computational complexity, longer iteration times and lower robustness where rapid variations in model parameters are involved, they were not adopted in the present study. In view of these considerations and the successful implementation of the basic LMS in suppressing biodynamic disturbances in manual control, Velger et al.^{13,14}, the extended LMS was used in the work described here.

The extended LMS filter

Figure 2 describes the basic LMS filter in conjunction with the variables and parameters described in Sec 2 above and in its role of noise suppression. The error, e_j , which drives the algorithm is given by

$$e_j = U_{c_j} + U_{b_j} - \hat{U}_{b_j} = U_{c_j} - \tilde{U}_{b_j} \quad (1)$$

j is the index of the sampled process. The estimation error \tilde{U}_b is given by

$$\tilde{U}_{b_j} = U_{b_j} - \hat{U}_{b_j} \quad (2)$$

U_c adds to e and upsets the proper convergence of the algorithm. Therefore, in order to assure $\hat{U}_b \rightarrow U_b$, it is necessary to fulfill the condition that $U_c \ll U_b$. Assuming that the parameter variations of the human biodynamic model are relatively slow and small, \hat{U}_b converges to U_b with satisfactory precision. The filtered signal U_f therefore is given by:

$$U_{f_j} = U_{c_j} + U_{b_j} = U_{c_j} + \tilde{U}_{b_j} \approx U_{c_j} \quad (3)$$

Equation (3) indicates that the biodynamic interference due to a is essentially canceled. In reality, the condition $U_c \ll U_b$ is not fulfilled. U_c can be in the order of 90 deg or more, while U_b is normally in the order of 1 deg. The variations in the parameters of the human biodynamic model are not necessarily slow. They may be rather rapid as a result of sudden changes in posture or muscle tone. Therefore, the basic filter, as shown in Fig. 2, does not meet all the requirements. The extended LMS filter, which can estimate both U_b and U_c , is shown in Fig. 3. A high-pass filter, for example of the type $s/(s+k)$, is inserted both in the Y_b and the AF path in order to maintain proper phase balance. The error e now is

$$e_j = \frac{s}{s+k} (U_{t_j} - \hat{U}_{b_j}) = \frac{s}{s+k} (U_{c_j} - \tilde{U}_{b_j}) \quad (4)$$

Thus, with the high-pass filters, e is affected by changes in U_c and not by U_b itself. Consequently, the estimated gradient is given by

$$\hat{\nabla}_j = 2e_j \frac{\partial e_j}{\partial \underline{w}_j} = -2e_j \left\{ \frac{s}{s+k} \underline{x}_j \right\} \quad (5)$$

And the extended LMS algorithm takes the form

$$\underline{w}_{j+1} = \underline{w}_j + 2\mu_j e_j \left\{ \frac{s}{s+k} \underline{x}_j \right\} \quad (6)$$

Where \underline{x}_j represents the accelerations a_j , μ_j is the gain and \underline{w} is the weight vector. In the actual implementation, a is high-pass filtered in order to reduce the effects of sensor bias and gravity.

The estimate of the nonvoluntary head motion \hat{U}_b is

$$\hat{U}_{b_j} = \underline{w}_j^T \underline{x}_j \quad (7)$$

and the estimate of the voluntary head motion U_f is

$$U_{f_j} = U_{t_j} - \hat{U}_{b_j} = U_{c_j} + \tilde{U}_{b_j} \quad (8)$$

In order to assure that the convergence rate of the algorithm is independent of the input intensity \underline{x} , μ_j is chosen such that

$$\mu_j = \frac{1}{f \text{tr}(R_j)} \quad (9)$$

where f is a constant coefficient $f > 1$ and R is the covariance matrix of the input \underline{x} . This choice of μ_j yields the Normalized LMS (NLMS). The spread of the eigenvalues of R is reduced by the square root of the spread as compared to the basic LMS algorithm. The rate of convergence and its sensitivity to eigenvalue spread are substantially reduced, Honig and Messerschmitt¹².

Rapid adaptation requires a large μ . In accordance with Eq. (9) this implies a small f . The smaller f , the larger the misadjustment noise in the estimated weight vector \underline{w} , Widrow and McCool¹⁰. On the other hand, the smaller μ , the slower the adaptation rate. A remedy to this conflict is to implement an error dependent $\mu = \mu(\epsilon)$, where $\mu(\epsilon)$ is a monotonic function in ϵ independent of $\text{sgn}(\epsilon)$. Thus, if ϵ , for example, increases as a result of a change in Y_b , μ is large and the adaptation is rapid. Yet, once convergence proceeds, μ becomes small, and the misadjustment noise becomes small. The implementation of μ is as follows: We choose μ_0 in accordance with the stability criterion of the algorithm, Widrow and McCool¹⁰, namely

$$\mu_0 = \frac{1}{f \text{tr}(R_j)} \quad (10)$$

We define:

$$\underline{e}_j \triangleq [e_j, e_{j-1}, \dots, e_{j-(N'-1)}]^T \quad (11)$$

where $N' > N$

let

$$\underline{e}_j^2 \triangleq \underline{e}_j \underline{e}_j^T = \sum_{i=j-(N'-1)}^j e_i^2 \quad (12)$$

$$\epsilon_j \triangleq \left[\frac{\underline{e}_j^2}{\text{tr}(R_j)} \right]^{1/2} \quad (13)$$

a possible method to implement $\mu(\epsilon)$ is: We define threshold and saturation values ϵ_t and ϵ_s and we prescribe,

$$\mu_j(\epsilon) = \begin{cases} 0 & 0 \leq \epsilon_j < \epsilon_t \\ \frac{\epsilon_j - \epsilon_t}{\epsilon_s - \epsilon_t} \mu_{0j} & \epsilon_t \leq \epsilon_j < \epsilon_s \\ \mu_{0j} & \epsilon_s \leq \epsilon_j \end{cases} \quad (14)$$

However, large angular head motion, in spite of the high-pass filter $s/(s+k)$, will still cause large transients in e and perturbations in \underline{w} . In order to overcome this problem, we set $\mu_j(\epsilon)=0$ whenever the error e exceeds a given threshold e_0 . We divide e into two components, namely e_c resulting from large head motion, and e_b , resulting from the nonvoluntary head motion. Thus,

$$e_j = e_{c_j} + e_{b_j} \quad (15)$$

Whenever $|e_j| > e_0$, $\mu_j(\epsilon) = 0$ and \underline{w} is frozen. e_0 is so chosen that $\text{Prob}\{e_j \geq e_0\} \rightarrow 1$ whenever the variations in U_c are large. When the variations in U_c are small, the threshold e_0 must fulfill the condition $\text{Prob}\{e_{b_j} \geq e_0\} \rightarrow 1$. The advantage of freezing the weights is, that after a large change in U_c , only a short time is needed to re-establish a good estimate of U_b . The disadvantage is that during the freezing intervals, parameter tracking is inhibited.

Bias and g components in the accelerometers degrade the convergence of the algorithm and cause errors in the estimate of U_b . This can be overcome by additional high-pass filtering of the accelerometer readings.

Choice of Adaptive Filter Parameters

Three principal parameters are involved:

1. The number of weights N .
2. The length of the delay sequence of the filter, T_f , in terms of real time as defined in Eq. (16) below.
3. The length of the delay interval between samples ΔT .

These parameters are related by

$$T_f = (N-1) \Delta T \quad (16)$$

Since normally $N \gg 1$, we have:

$$N = \frac{T_f}{\Delta T} \quad (17)$$

In order to ensure proper performance of the algorithm, T_f must be longer than the effective length of the infinite impulse response (IIR) of Y_b . This value is usually not known. However, a rough estimate can often be made and T_f can be assigned with some excess margin. The average time constant of convergence of the filter in terms of the number of iterations, τ_{it} , for the adaptation error to decay to e^{-1} of its original value, in accordance with Widrow et al.¹⁵, is shown to be determined by:

$$\tau_{it} = \frac{fN}{4} \quad (18)$$

In order to ensure a convergence error not greater than 2% of its initial value, the number of iterations τ_{it} which is required, is $4\tau_{it}$. Therefore, the convergence time constant τ_s is proportional to T_f in accordance with

$$\tau_s = f \left(\frac{T_f}{\Delta T} + 1 \right) \Delta T \approx fT_f \quad (19)$$

The sampling interval ΔT must comply with the sampling theorem i.e.,

$$\Delta T \leq \pi/\omega \quad (20)$$

where ω is the bandwidth of the input signal $x(t)$.

In addition to the requirement imposed by the sampling theorem, the number of weights N must be sufficiently large so that the Finite Impulse Response (FIR) approximation describes with sufficient fidelity the actual IIR of Y_b . For example, if the IIR contains periodic modes, N must be able to provide at least six samples per period $T = 2\pi/\omega$.

Another factor to be considered is the misadjustment factor, M , which is defined as the excess parameter noise in \underline{w} over the noise in the asymptotic Wiener solution of the LMS, Widrow et al.¹⁵. The misadjustment, M , is given by

$$M = 1/f \quad (21)$$

It is therefore clear that a large value of f reduces M , but increases the number

of iterations in accordance with Eq. (18). f is therefore chosen as a compromise between these conflicting factors by trial and error and so are the parameters ϵ_s and ϵ_t in $\mu(\epsilon)$ and the threshold value e_0 .

4. Computer Simulations

In this section a number of computer simulations of the performance of the adaptive filter with a linear model for Y_b are described. This model was developed with the aid of preliminary experiments. A human subject placed in the moving base simulator was sinusoidally vibrated in the vertical axis at frequencies up to 10 Hz. It was found that in the neighborhood of 5 Hz, Y_b exhibits a resonance with a peak of 12 dB. At frequencies below 1 Hz and above 7 Hz, no significant head motion was observed. These findings are substantiated by previous studies, Griffin¹⁶. It follows that $Y_b(s)$ has at least one zero at $s=0$ and that it sharply cuts off beyond 7 Hz. The transfer function which was obtained by a fitting procedure, closely describes the experimental results, and is given by:

$$Y_b(s) = 3160000 \frac{s^2}{(s+20)^4 (s^2 + 19s + 990)}$$

Figure 4 illustrates the impulse response corresponding to $Y_b(s)$.

The Adaptive Filter used in the Simulations

Figure 5 demonstrates that the effective length of the IIR of Y_b is about 0.6 sec. The sampling rate in the experimental set up is 37 msec. This rate was also chosen for the computer simulations. N was set to 30 in order to provide acceptable fidelity and to avoid FIR truncation due to insufficient length T_f which was set to 0.81 sec. The high-pass filter $s/(s+k)$ was set to have a break point at 1 Hz. The other filter parameters were chosen in accordance with the guidelines in section 3 and by a cut and try approach. Thus, the following values were chosen: $f=2$; $\epsilon_s = 0.001$; $\epsilon_t = 0.0011$; $\epsilon_0 = 0.5$. The initial conditions were: $\underline{y} = 0$; $\underline{x} = 0$.

Suppression of Interference with Small Head Motion

The purpose of this simulation is to test the performance of the algorithm in the simple case of small voluntary head motion U_c . The simulated vertical acceleration which excited the model, $Y_b(s)$, was obtained by passing Gaussian white noise through a second order low-pass filter with a cut-off frequency of 30 Hz and a damping factor of 0.5. The nonvoluntary head motion U_b , which resulted from this excitation is described in Fig. 5a. Figure 5b shows that the estimation error \tilde{U}_b is less than 1% of U_b . This result demonstrates the high estimation precision which can be obtained. In this example, since $U_c = 0$, $U_f = \tilde{U}_b$. The square of the convergence error, e^2 , is shown in Fig. 5c. The convergence history of three of the weights is shown in Fig. 5d. These two figures indicate that the convergence time is about 7 sec which permits on-line operation. Figure 5d also demonstrates the small misadjustment noise achieved by the algorithm. Figure 4 which compares the estimated FIR of Y_b , which consists of the values to which the 30 weights of the algorithm have converged, with the IIR describing $Y_b(s)$, demonstrates their excellent correspondence.

Suppression of Interference with Large Head Motion

In this example the acceleration a and U_b are the same as in the foregoing example. Now, U_c adds to U_b and it is shown in Fig. 6a along with U_t . Figure 6b shows U_c along with its estimate U_f . Figure 6c demonstrates that during large variations in U_c , \tilde{U}_b is about 0.75 deg peak-to-peak. It constitutes about 3.75% of estimation error of U_c , and about 37% of U_b . Figure 6d demonstrates the rapid reconvergence of the weights after the transient of the large head motion U_c is over, and their freezing during the transient provided by the freezing logic described in Sec 3.

The purpose of this simulation is to investigate the performance of the adaptive filter in the presence of sudden model parameter jumps. In this example, the gain of the model $Y_b(s)$ was increased by 50%, at 15 sec after the beginning of the simulation run which was started as described in the foregoing example. Figure 7 demonstrates the jumps in the weights and their reconvergence to their new values within about 4 sec. The comparison of FIR with the IIR of the model after the 50% gain jump demonstrates an excellent fit.

Offsets in the accelerometer cause an increase in convergence time of the algorithm and they may even prevent proper operation of the filter. The increase in convergence time is a result of the settling time of the high-pass filter $s/(s+k)$. An additional high-pass filter, located in both AF and $Y_b(s)$ paths with a break frequency in the order of magnitude of 0.5 Hz, ensures proper convergence of the algorithm, however with a slight increase of 15% in \bar{U}_b .

To achieve proper convergence of the weights \underline{w} in the LMS filter, it is necessary to assure a sufficiently wide band excitation signal of Y_b . In the real environment of the aircraft this condition is normally not met. With narrow band excitation, the adaptation error, e^2 , still converges to zero, but \underline{w} will normally not converge to the correct values. This, however, does not prevent precise estimation of U_b and U_f which only requires the vanishing of e^2 .

The modeling, filter design and computer simulation, described in this section indicate that the methodology of adaptive noise cancellation has the potential to adapt to rapid parameter variations, and to identify U_b in the presence of large values of U_c . This, however, must be validated by actual man-in-the loop experiments which are described in the next section.

5. Experimental Validation.

The purpose of the experimental validation described in this section is to examine the validity of the assumed model $Y_b(s)$ and to study the performance of the adaptive filter with real human subjects and in the real physical environment of a vibrating platform driven by signals similar to actual helicopter vibration spectra, and which includes unknown nonlinearities, such as in the seat, or additional noise and imperfections in the accelerometers, head motion sensor and display systems. In the experiments it was not yet possible to directly validate the suppression of display blurring for the following reasons:

- i. The lack of a helmet mounted display with the necessary resolution which permits the display of sufficiently small characters and symbols for which blurring becomes significant.
- ii. Limitations in the sampling rate of the head motion sensor and the display system which amounted to 40 msec and caused phase shifts in the order of 70 deg at typical vibration frequencies in the region of 5 Hz. Such phase shifts prevent effective image stabilization as outlined in section 2.

In spite of these present shortcomings, it was possible to put together a simulation set-up for man-in-the loop experiments. This set-up incorporates the following subsystems:

1. Six-degrees-freedom simulator.
2. Cabin mounted accelerometer.
3. System for measuring head motion in six-degrees-of-freedom.
4. A light air force type helmet equipped with the head motion sensor.
5. A *Digital VAX 750* computer.
6. A *Motorola VME System 1131* computer.
7. A *TV Barco* display generation and projection system.
8. Interfaces for sampling and communication between subsystems.

This set-up can also emulate the function of a helmet mounted display or

sight in its roles in head target tracking and pointing which also underlie the functions of head teleoperation.

Viewing Experiments

Subjects, seated in the simulator cabin one at a time, were instructed to carry out the following tests:

1. View freely a fixed point on the cabin panel to ensure small head motion.
2. Execute large head motion in elevation starting and returning to the fixed point.
3. While viewing the fixed point, change posture and tighten and relax muscles to cause variations in Y_b .

The cabin was vibrated at accelerations up to 0.33g and up to frequencies of 10 Hz. The vibration consisted of sums of sines and/or of a Gaussian white process filtered by a second order low-pass filter with various cut-off frequencies. Each run lasted 90 seconds. The first 15 seconds were assigned for the convergence of the adaptive filter and for proper settling in the seat. During the remaining 60 seconds the test was carried out. Data were recorded for the last 75 seconds. The recorded data were cabin accelerations and head motion. The signals served as the inputs to the adaptive filter that was operating in real time and its parameters and outputs were also recorded. Ten subjects participated in these tests.

The Adaptive Filter

The parameters of the adaptive filter were chosen in accordance with the computer simulations described in sec. 4. The length of the filter T_f , in accordance with Y_b described in sec. 4 was set to 0.81 sec. The sampling frequency was 37 Hz so that $\Delta T = 27$ msec, and the number of weights was set to $N = 30$. The threshold value was set to $e_0 = 1$ and the break frequency of the high-pass filter for U_t was set to 2.4 Hz.

Results of Viewing Experiments

Three examples, demonstrating the performance of the adaptive filter are given for the three different tests. The vibration conditions for the examples shown for tests one and two were sinusoidal vertical vibrations at 5 Hz with an amplitude of 0.156 g rms, and in the example given for the third test the subjects were vibrated sinusoidally at 5 Hz and 0.069 g rms. During all the tests the subjects viewed a fixed point on the panel.

Interference Suppression without Large Head Motion

Figure 8a demonstrates the rapid convergence of e^2 in the adaptive filter which permits good estimates of U_b and U_c . Figure 8b describes \hat{U}_b , which is about 0.5 deg peak-to-peak and, as anticipated, is at 5 Hz. It is accompanied by low frequency interferences which are due to small uncontrollable head motion. Figure 8c shows $U_t = U_c + U_b$. The 5 Hz component U_b is clearly visible along with the small variation of U_c . Figure 8d, demonstrating U_f , shows that U_b has almost been entirely removed without affecting U_c . The gradual drift downwards is due to a slow unintentional head motion which cannot be prevented in the simple viewing experiment described here and which does not incorporate a reticle which could have prevented this drift. For vibration tests with two or more sines and/or a random component, not shown here, the performance of the filter was comparable with the results shown in Figs. 8. In all examples of vibration, the adaptive filter is effective in identifying U_b even though the excitation of the human body is not rich and Y_b is not well represented by the corresponding FIR. The decisive factor in identifying U_b is the good convergence of e^2 .

Interference Suppression with Large Head Motion

Figures 9 shows the performance of the extended LMS adaptive filter in the presence of large head motion. The vibration was at 5 Hz and 0.23 g rms. Figure 9a shows a 15 sec section of large head motion U_c accompanied by the small 5 Hz vibration. Figure 9b shows U_t and that U_b has almost entirely been removed.

Interference Suppression with Parameter Variations in Y_b

Subjects were vibrated at 5 Hz and 0.069 g rms. At the instant $t = 30$ sec, the subject suddenly changed his posture from erect leaning to forward crouching without contact of his back with the chair support while tightening his torso and limb muscles as hard as he could. After 10 sec, the subject returned to his original posture. Again, the subject was instructed to view the fixed point on the panel. The history of e^2 demonstrates the sensitivity of the filter to the parameter variations, its rapid adaptation to this change and the rapid re-adaptation at 40 sec as expected. Figure 10 shows the corresponding variations of w_5 and w_{15} . It also shows that after about two seconds, the weights reconverge to almost their original values. The results also demonstrate that during the crouching posture the parameter noise is larger than during the erect posture, probably because it is more difficult to maintain constant levels in muscle tone in the crouching position with tightened muscles.

Comparison of the weights' time histories in Fig. 10 with those of the analytical model in Fig. 7, shows that in reality, the weights vary all the time, clearly, because of the persistent variations in posture and muscle tone.

6. Conclusions

The results shown in this paper demonstrate that the extended Least Mean Square filter estimates U_c and U_b rapidly and precisely. In view of the very small value of \tilde{U}_b/U_b , the application of the algorithm to actual helmet display systems, strongly indicates that display blurring due to vibration can be eliminated with the proposed filter algorithm. Very good performance has been demonstrated also in the presence of very large and sudden head motion and changes of posture and muscle tone. The analytical model proved very useful in the choice of the design parameters of the adaptive filter. The results also demonstrate that the image stabilization method based on adaptive filtering does

not entail lengthy transients after a large head motion or parameter variation. A general conclusion is that the methodology of Least Mean Square filtering is sufficiently robust to withstand the discrepancies between the actual dynamics involved and the linear model used in the computer simulations. Clearly, the results demonstrate that the algorithm is directly applicable in the improvement of precision in tracking and pointing in head teleoperated devices. Very good agreement was found between the real system, involving human subjects and numerous nonlinearities, and the linear model assumed in the concept development.

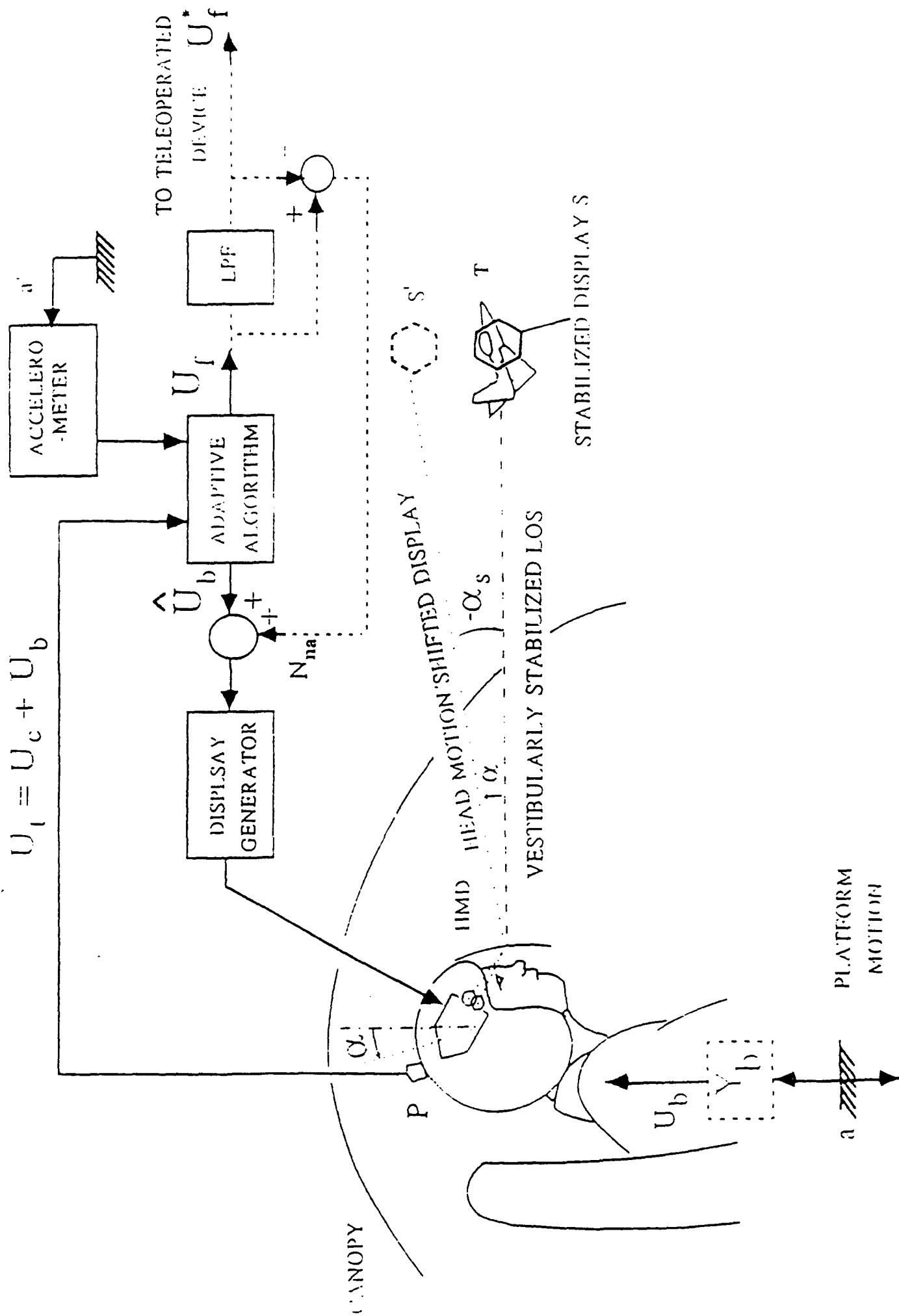
7. Acknowledgements

This work has been supported in part by the Human Factors Division, NASA Ames Center and by the USAF Aerospace Medical Research Laboratory, WPAFB, under grants NAWG 1128 and AFOSR88 0298, respectively.

8. References

1. Levison, W.H., Baron, S. and Junker, A.M., "Modeling the Effects of Environmental Factors on Human Control and Information Processing," Wright-Patterson Air Force Base, Ohio, AMRL-76-74, August 1976.
2. Jex, H.R., "Problems in Modeling Man Machine Control Behavior in Biodynamic Environments", *Proc. 7th Annual Conf. on Manual Control*, NASA SP-281, 1971.
3. Wells, M.J. and Griffin, M.T., "A Review and Investigation of Aiming and Tracking Performance with Head Mounted in Sights", *IEEE Trans. on Systems, Man and Cybernetics*, Vol. SMC-17, No. 2, March-April 1987.
4. Wells, M.J. and Griffin, M.J. "Tracking with the Head During Whole-Body Vibration", *Training, Human Decision Making and Control*, J. Patrick and K.D. Duncan (Eds.), Elsevier Science Publishers, B.V. (North-Holland), 1988.
5. Lewis, C.H. and Griffin, M.J., "Predicting the Effects of Vertical Vibration, Frequency, Combination of Frequencies and Viewig Distance on the Reading of Numeric Displays". *Journal of Sound and Vibration*, 1980.
6. Wells, M.J. and Griffin, M.J., "Benefits of Helmet Mounted Display Image Stabilization Under Whole Body Vibration", *Aviation, Space and Environmental Medicine*, January 1984.
7. Benson, A.J. and Barnes, G.R., "Vision During Angular Oscillation: The Dynamic Interaction of Visual and Vestibular Mechanisms", *Aviation. Space and Environmental Medicine*, April 1978.
8. Wells, J.M. and Griffin, M.J., "Flight Trial of a HMD Image Stabilization System", *Aviation, Space and Environmental Medicine*, April 1987.
9. Merhav, S.J., "Adaptive Suppression of Biodynamic Interference in Helmet Mounted and Head Down Displays", *AIAA Guidance, Navigation and Control Conference*, Minneapolis, Minnesota, August 1988.

10. Widrow, B. and McCool, J.M., "A Comparison of Adaptive Algorithms Based on the Method of Steepest Descent and Random Search", *IEEE Trans. on Antennas and Propagation*, Vol. AP-24, No. 5, Sept. 1976.
11. Haykin, S., "Adaptive Filtering Theory", Book, Prentice-Hall Information Systems Science Series, 1986.
12. Honig, M.L., Messerschmitt, D.G., "Adaptive Filters, Structures, Algorithms and Applications", Book, Kluwer Academic Publishers, 1984.
13. Velger, M., Grunwald, A. and Merhav, S., "Suppression of Biodynamic Disturbances and Pilot-Induced Oscillations by Adaptive Filtering", *AIAA J. of Guidance, Control and Dynamics*, July-August 1984, pp. 401-409.
14. Velger, M., Grunwald, A. and Merhav, S., "Adaptive Filtering of Biodynamic Stick Feedthrough in Manipulation Tasks on Board Moving Platforms", *AIAA J. of Guidance, Control and Dynamics*, Vol. 11, No. 2, March-April 1988.
15. Widrow, B. et al., "Stationary and Nonstationary Learning Characteristics of the LMS Adaptive Filter", *Proceedings of the IEEE*, Vol. 64, No. 8, August 1976.
16. Griffin, M.J., "The Transmission of Triaxial Vibration to Pilots in the Scout AH MK1 Helicopter", University of Southampton, Institute of Sound and Vibration Technical Report No. 58, Southampton, August 1972.



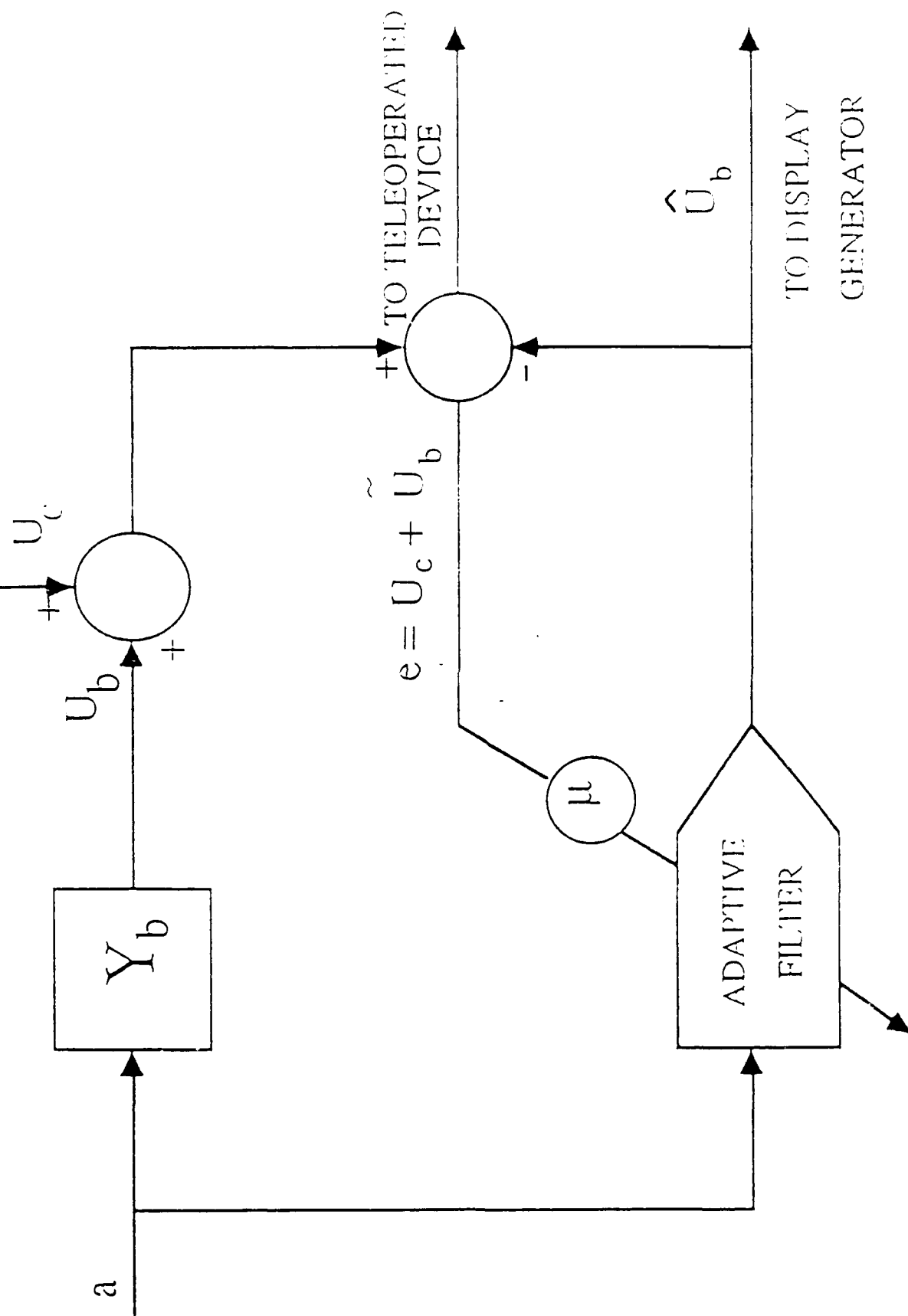


Figure 2. Basic LMS algorithm for suppression of biodynamic interference in HMD and head teleoperation.

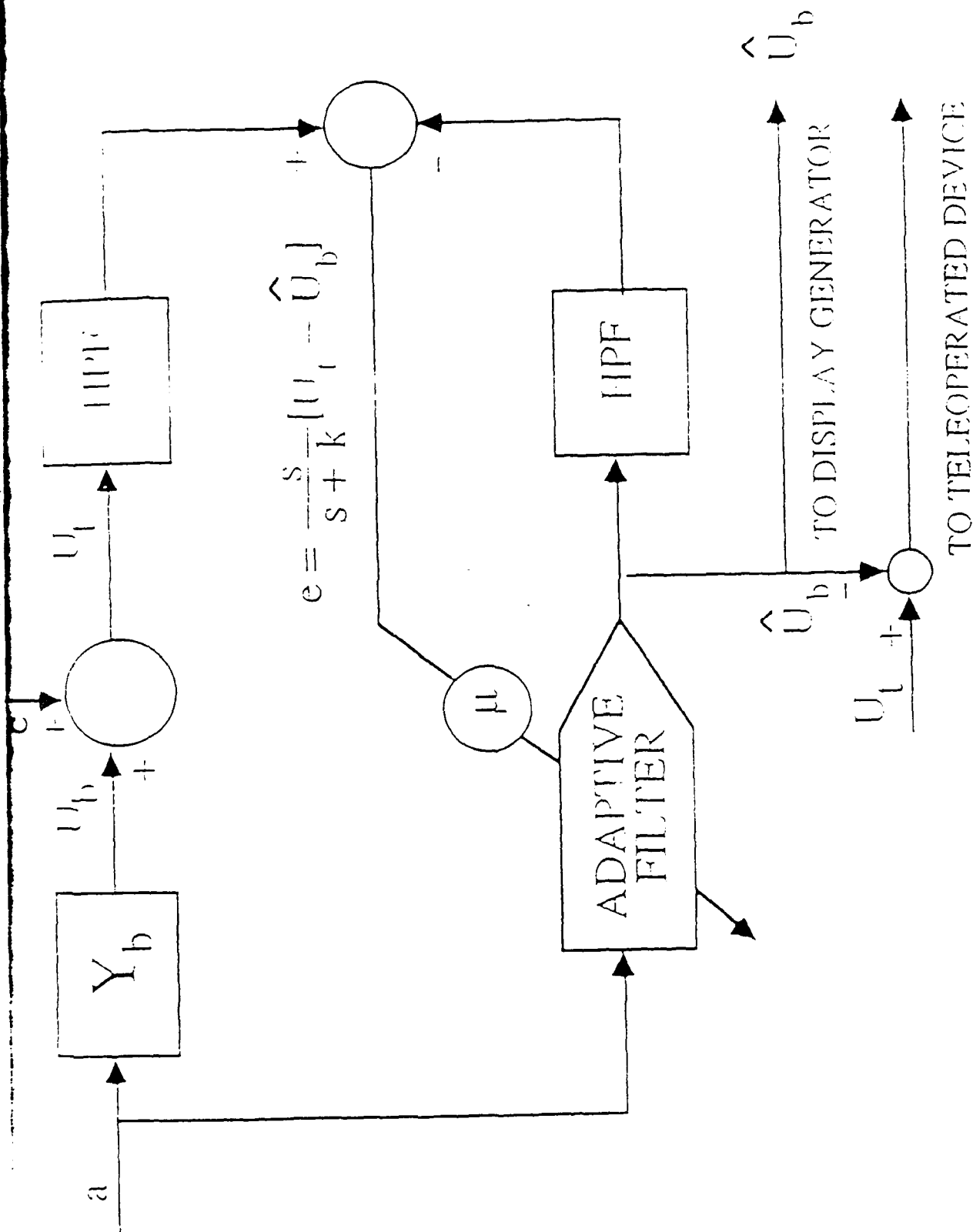


Figure 3. Extended LMS algorithm for suppression of biodynamic interference in HMD and head teleoperation.

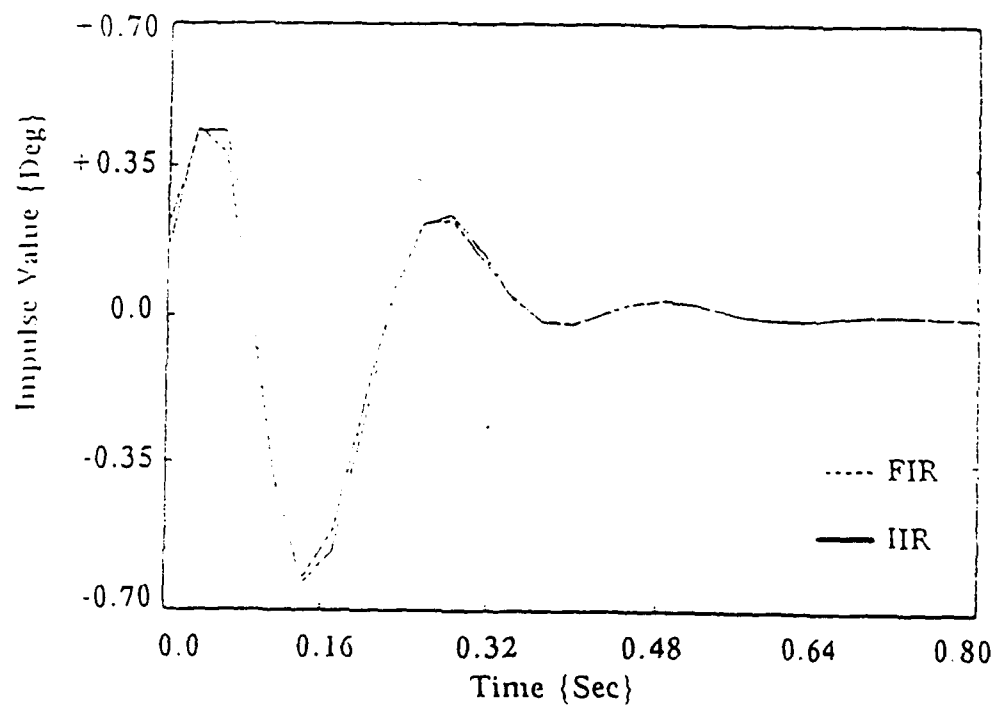


Fig. 4. FIR and IIR for the linear biodynamic model $Y_{b_L}(s)$.

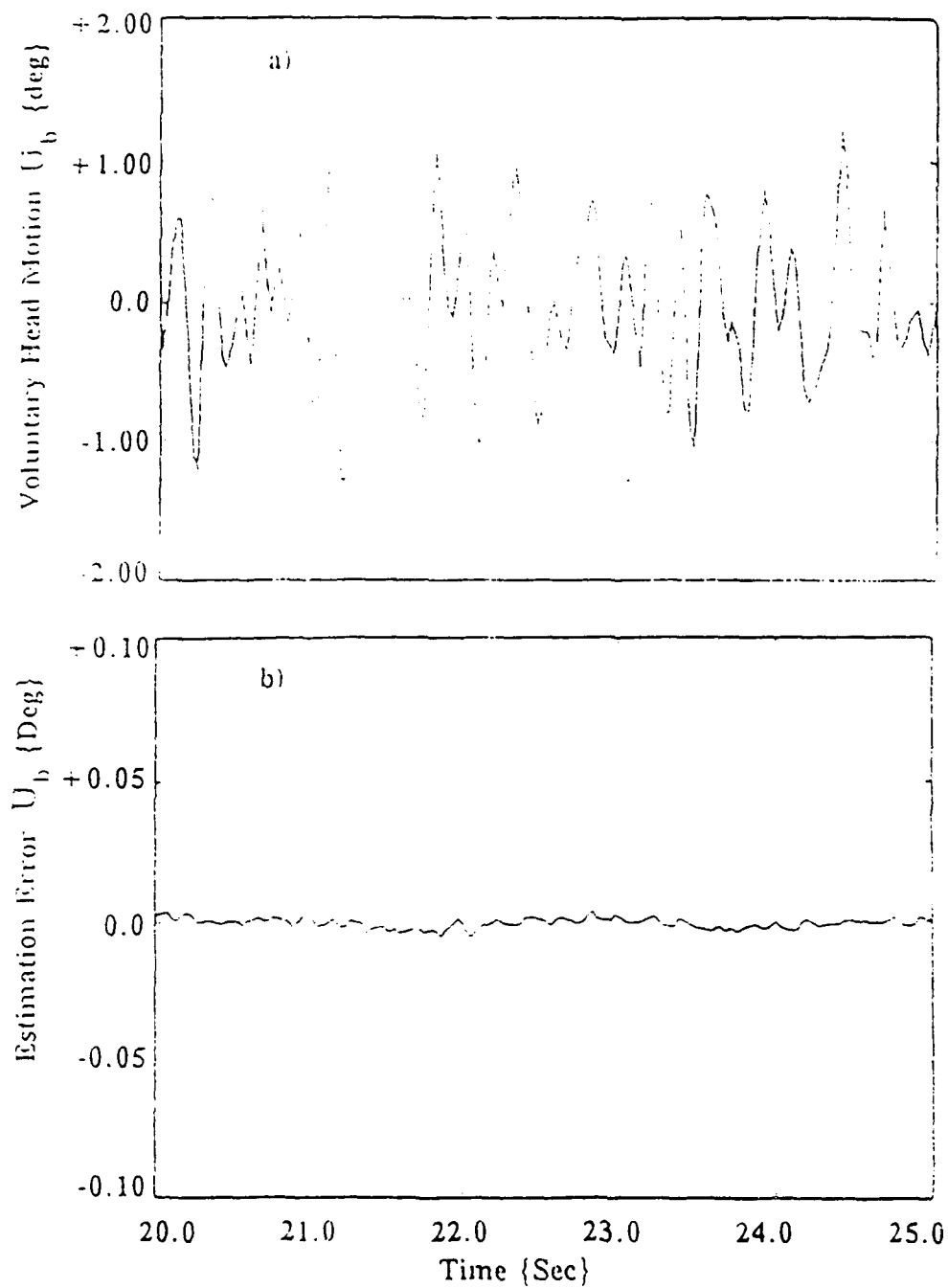


Fig. 5 (a,b) A section of the time history of a) nonvoluntary head motion; and b) estimation error \hat{U}_b for the example without large head movements

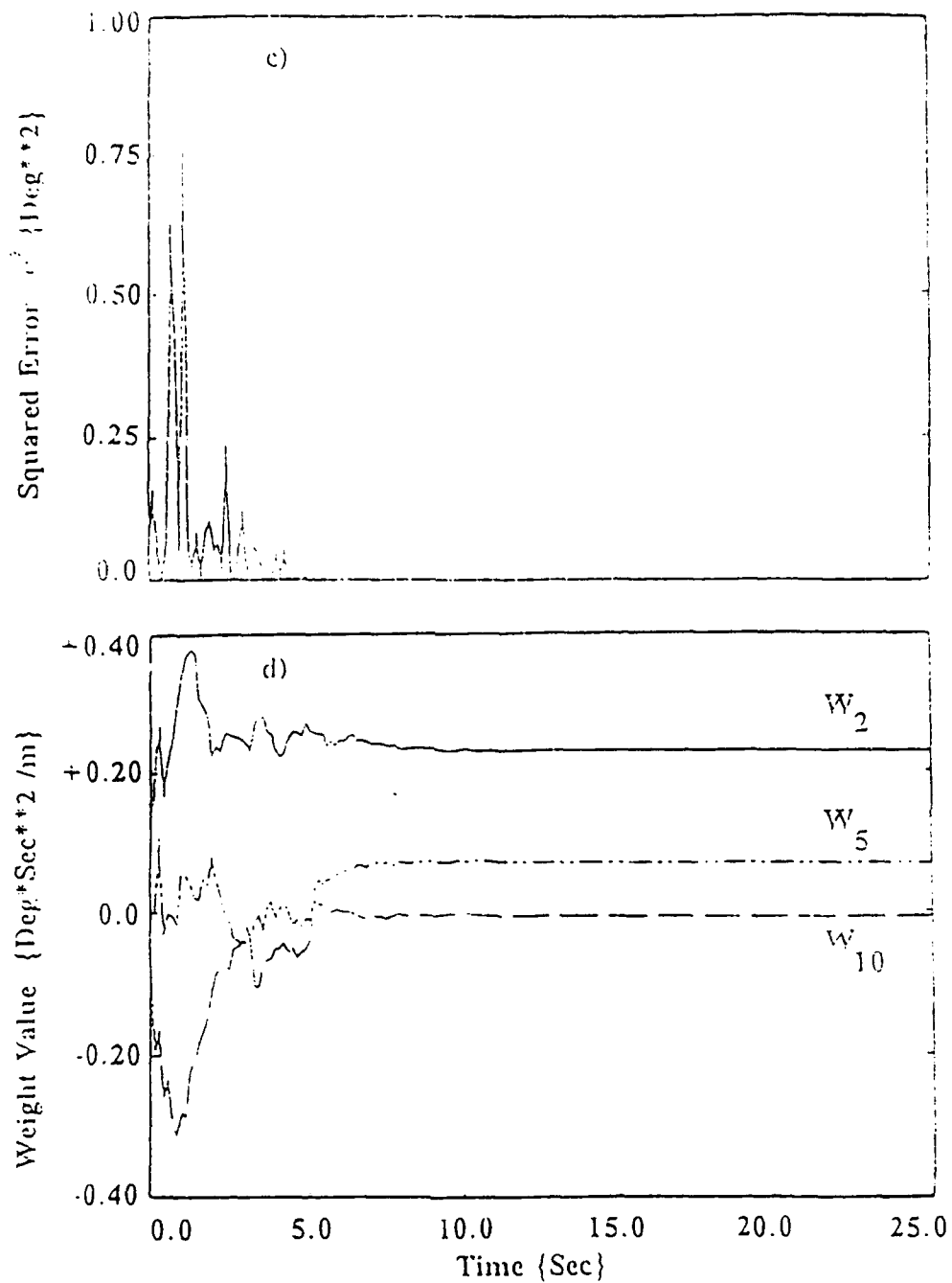


Fig 5 (c,d) A section of the time history of c) square of convergence error e^2 , and d) three of the weights for the example without large head movements

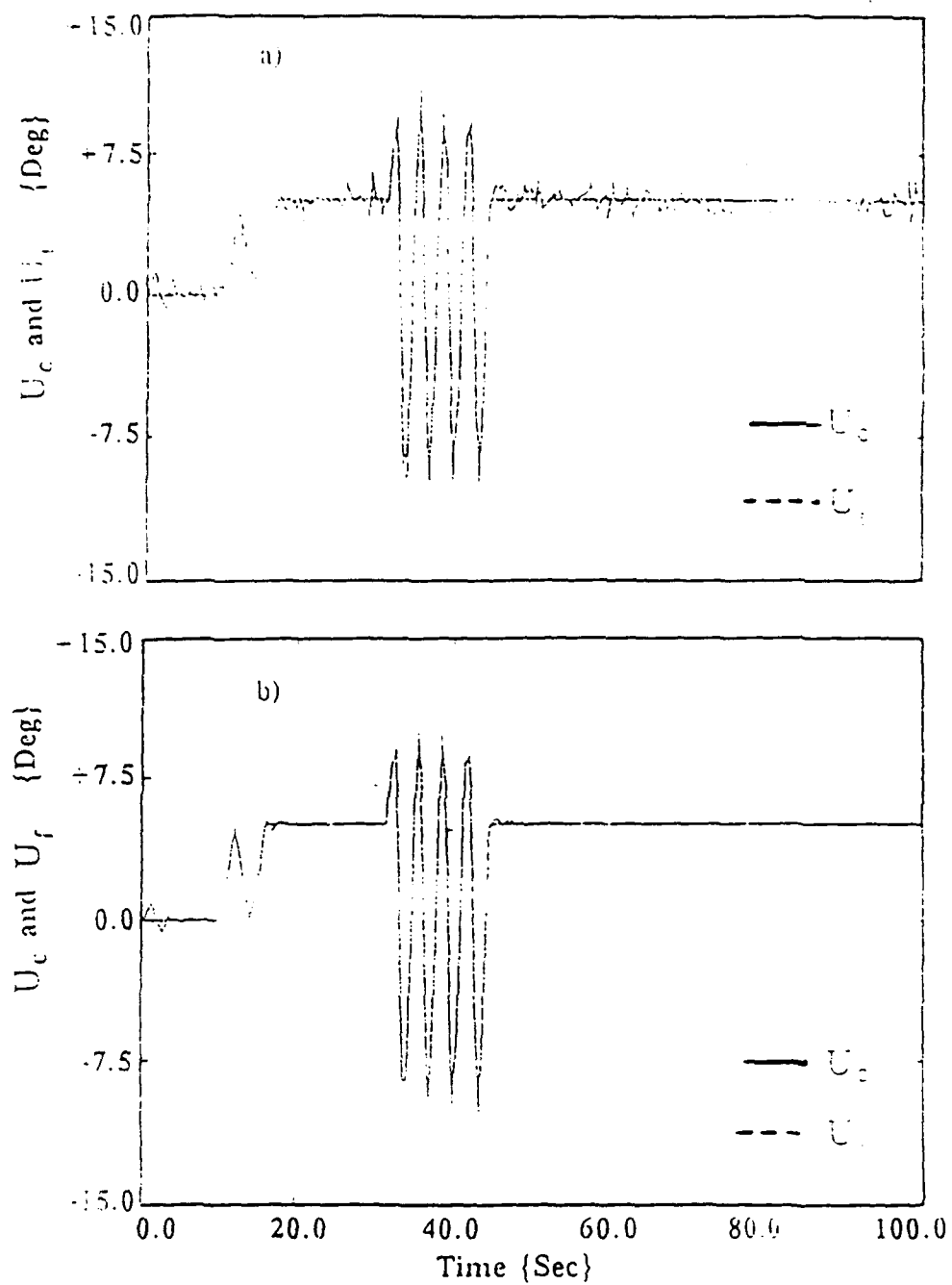


Fig 6 (a,b) Time history of a) total and voluntary head motion; and b) voluntary motion and its estimation, for the example with large head motion

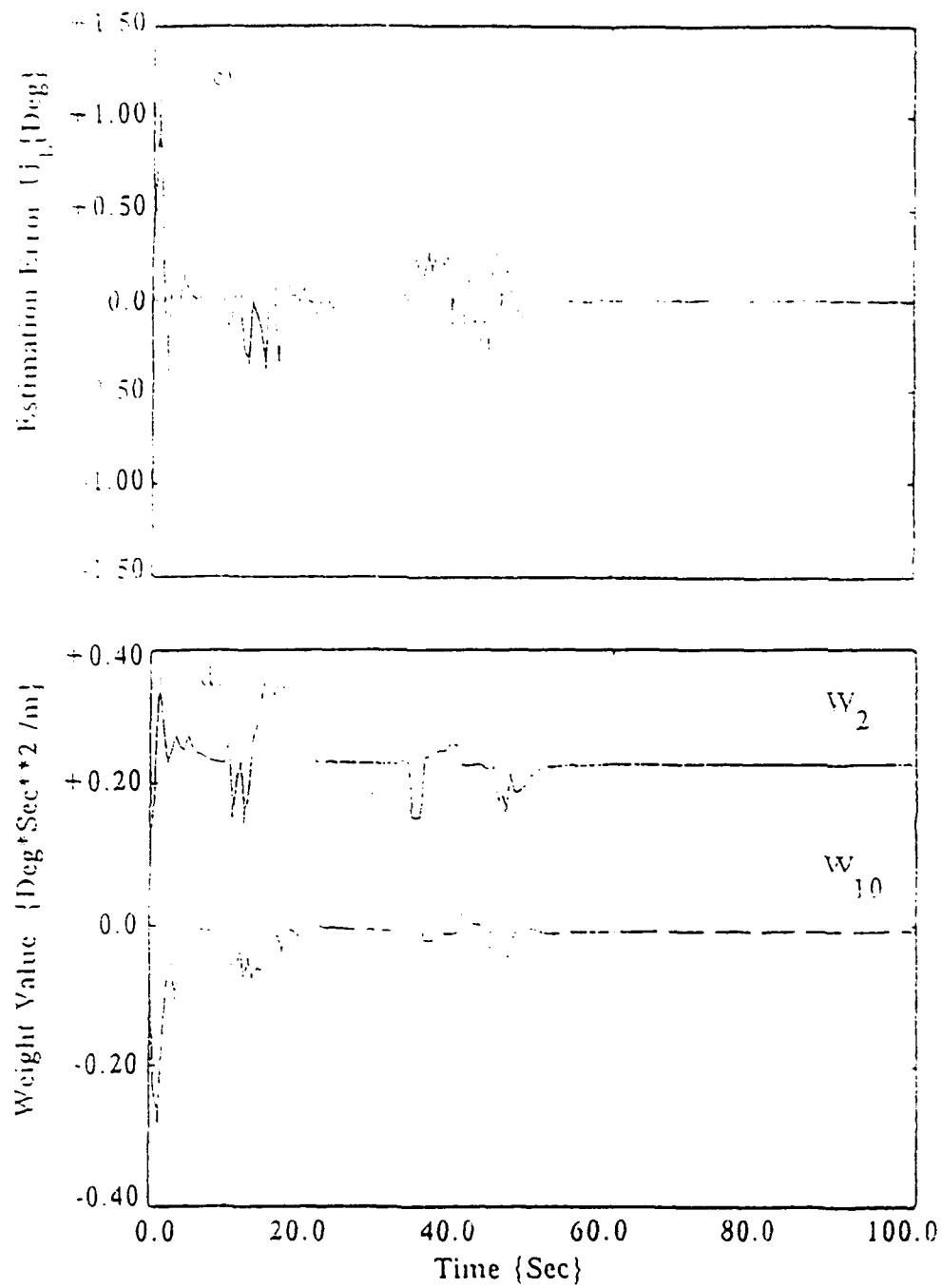


Fig. 6 (c,d) Time history of c) estimation error \hat{U}_j , and d) two of the weights, for the example with large head motion

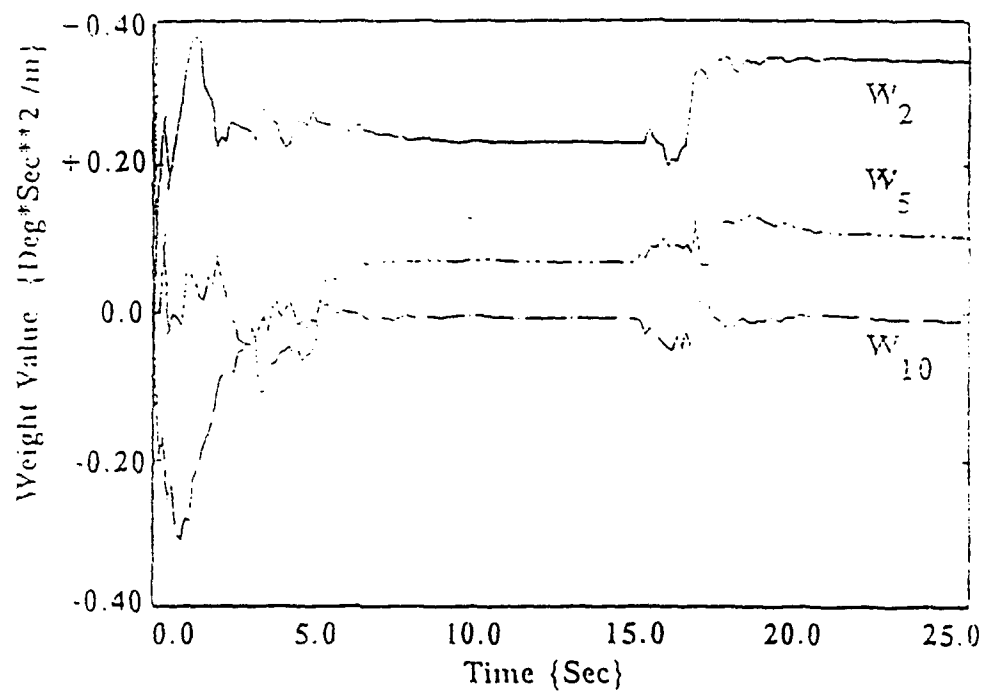


Fig 7. A section of the time history of three of the weights for the example with parameters jumps.

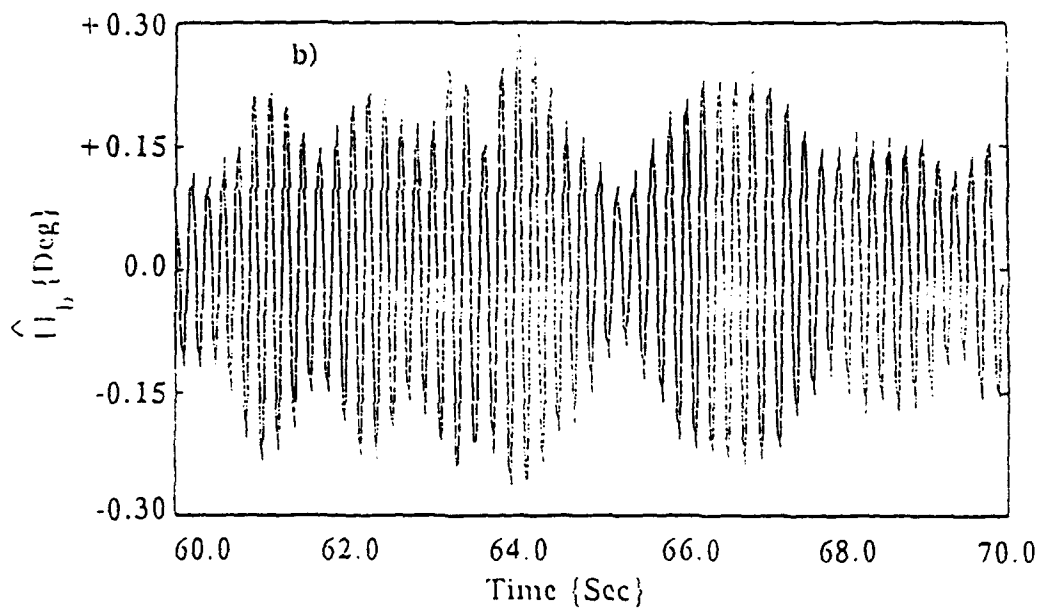
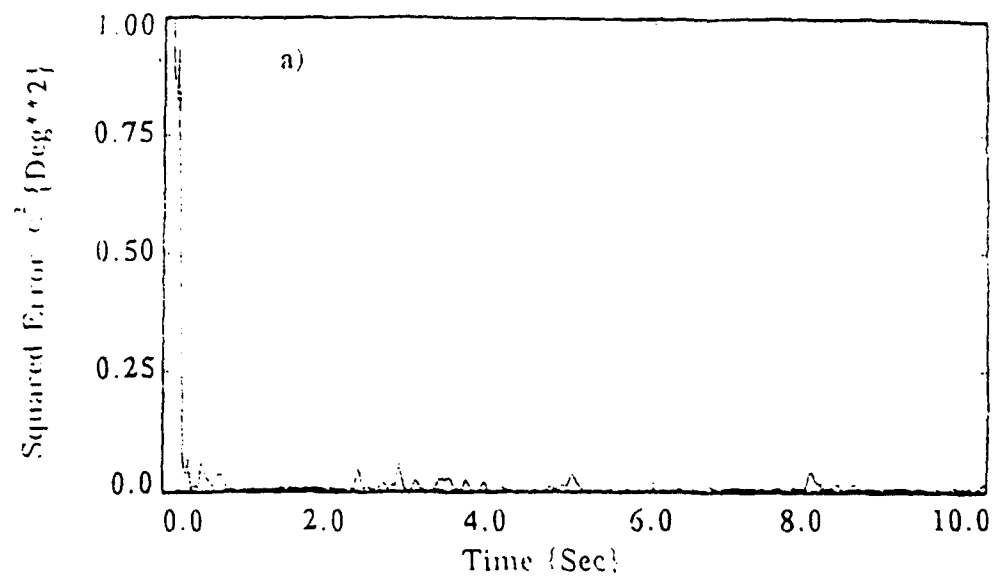


Fig. 8 (a,b) A section of the time history of: a) square of the convergence error e^2 , and b) estimated non-voluntary head movement \hat{U}_b , for the example with single sine excitation and without large head movement.

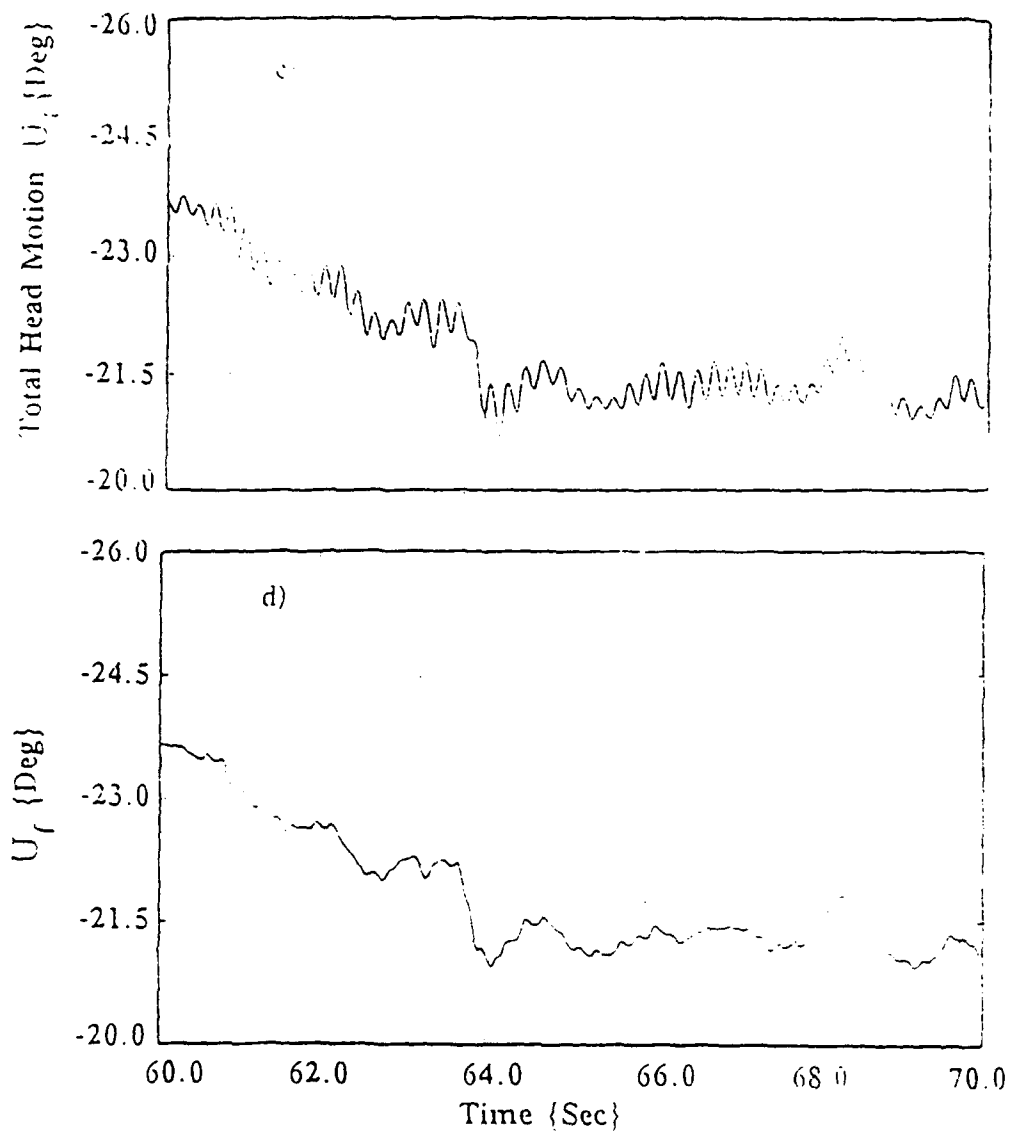


Fig. 8 (c) A section of the time history of total headmovement U_T , and (d) estimated voluntary head movement U_V , for the example with single sine excitation and without large head movement.

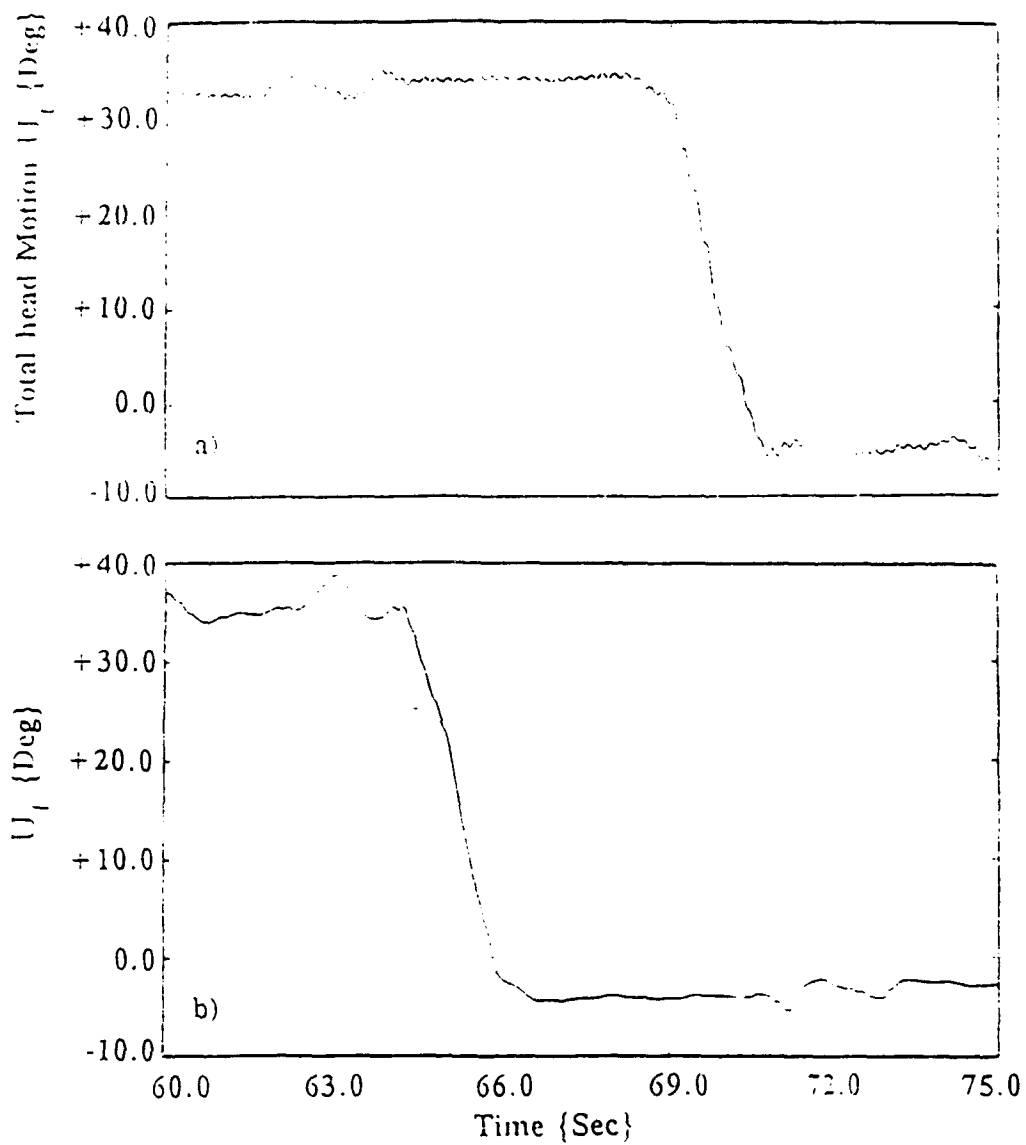


Fig. 9 (a, b): A section of the time history of a) total head movement U_T , and b) estimated voluntary head movement U_r , for the example with single sine excitation and large head movement.

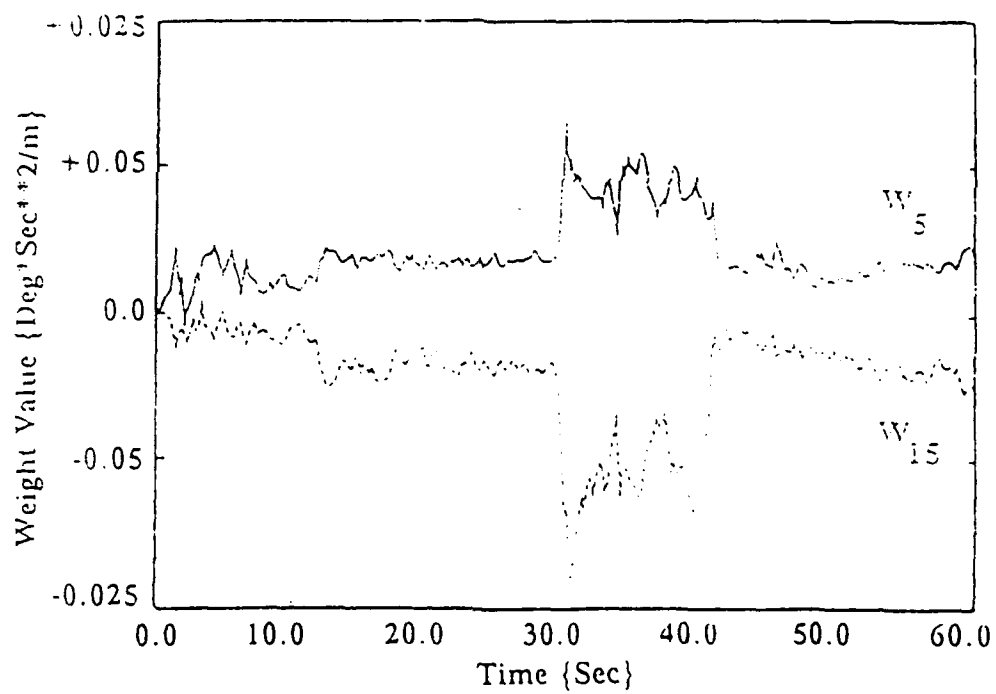


Fig 10. A section of the time history of two of the weights, for the example with single sine excitation and with changes in biodynamic parameters

MAN-IN-THE-LOOP STUDY OF FILTERING IN AIRBORNE HEAD TRACKING TASKS

S. Lifshitz[#] and S. J. Merhav^{*}

Department of Aerospace Engineering, Technion, Haifa Israel

Abstract

On Board head tracking of targets by means of Helmet Mounted Sights for teleoperation of cameras, lasers, or antennas is often subjected to dynamical interferences which affect the precision required in such tasks. These interferences, which result from aircraft motion and vibration, consist of an additive component correlated with the aircraft vibration and a nonadditive component known as remnant. In this paper, a simulation study is described in which improvements in pointing and tracking precision are investigated using dynamic display shifting by means of adaptive and low-pass filtering. The results indicate that substantial improvements of up to sixty percent can be achieved in percentage on-target dwelling time and tracking precision relative to tracking without filtering.

This paper is based on the M. Sc. thesis of the first author.

[#] Graduate student.

^{*} Professor, Head, Flight Control Laboratory

1. Introduction

Air combat and attack missions in modern warfare impose a heavy work load on the pilot.. A major technological goal is to reduce this work load by a Helmet Mounted Display (HMD) and by providing pointing and target tracking by means of head teleoperation. Aircraft vibration and buffetting tend to impair the proper performance of such systems. In this paper a method for reducing the effects of vibrations on the precision of pilot head pointing and tracking is investigated. Vibration causes biodynamic interferences, Levison¹ and Jex², which, in turn, cause vision blurring in HMD's, Wells and Griffin³ and Lewis and Griffin⁴, and degradation of tracking and pointing accuracy, Wells and Griffin^{5,6}. A method for reducing these effects by estimating in real time the nonvoluntary components of head motion and to use these signals to stabilize the symbols in the image plane of the display and, thus, to reduce blurring in viewing tasks has been described by Lifshitz and Merhav⁷. In this regard, a distinction must be made between viewing tasks and tracking tasks. In the viewing task the interference is additive and can be handled by noise cancellation methods. In the tracking task, however, the remnant noise increases with the intensity of the vibration and often becomes dominant. The remnant noise is not additive, and cannot be directly reduced by the noise cancellation method⁷. Therefore, additional filtering schemes are needed to reduce the effects of biodynamic interference. The Helmet Mounted Sight (HMS), enables head teleoperation of devices for pointing or tracking, Nicholson⁸. The helmet is equipped with a sensor which measures head orientation and position with respect to cockpit reference axes. The sight image, focused to near infinity, is projected onto a semi-transparent visor and it enables the acquisition and tracking of targets. The precision with which this can be accomplished is affected by the uncontrolled angular vibration of the head. The resulting tracking error was found to increase with the pilot work load, Grossman⁹. For sinusoidal vertical vibration at 4 Hz and the intensity of 0.14g rms, the angular tracking error was found to be 1.3 deg for a stationary target, Simpson et al.¹⁰. For a maneuvering target, and simulated Cobra flight,

the angular tracking error was found to be 0.77 deg rms, Verona¹¹. Wells and Griffin⁵ divided the factors which influence tracking precision into three categories, namely:

1. Minor effects: Apparent target size, the shape of the reticle, right or left eye, seat type, helmet weight, elevation of line of sight, nature of secondary task.
2. Significant effects: Size of the reticle, azimuth of line-of-sight.
3. Major effects: Head vibration, target motion.

Wells and Griffin⁶ investigated, under laboratory conditions, by means of a helmet sight, the effects of head vibration and target motion on the tracking error. The most pronounced increase in tracking error was in the region 3 - 5Hz, which is where the biodynamic feedthrough from seat to head and the remnant non-additive component of biodynamic interference; were the largest. The effects of atmospheric turbulence on tracking precision were investigated by Tatham¹² in a series of flight tests and simulations. The tests were performed with a Canberra aircraft at the speed of 350 knots and an altitude of 350 ft.. The vibrations were recorded and replayed in simulation tests. The frequency range was between 0.5 to 25 Hz, and the acceleration intensity was 0.25 g and 0.1 g in the vertical and horizontal axes respectively. Under these conditions the tracking error was 1.72 deg rms in elevation and 0.92 deg rms in azimuth. Tatham¹² attempted three methods to improve tracking precision:

1. Low-pass filtering of the head motion signals which control the teleoperated device. This resulted in a 50% decrease in tracking error, but, at the expense of a phase lag which, in the absence of actual visual feedback from the teleoperated device, causes it to lag behind the head motion, thus, increasing the actual tracking error.
2. The pilot was instructed to indicate the instance, when in his judgment, he succeeded to align the reticle with the target. At this instant, the tracking error was automatically determined and recorded by the experimental system. No improvement was noticed.

3. In the simulation experiments, the gearing ratio between angular head motion and angular target motion was varied from one to ten. Thus, a larger signal to noise ratio (voluntary to non-voluntary) was achieved. The results indicated better performance for the larger ratios. However, this approach is not realistic for actual transparent helmet sights, and, it requires excessive angular head motion.

The method presented in this paper for improving aiming accuracy in tracking tasks is based on head motion measurement and on the shifting of the reticle in the HMD, in such a way as to inhibit much of the nonvoluntary apparent motion of the reticle relative to the target and the nonvoluntary motion of the teleoperated device. The HMD also inherently provides the required visual feedback.

Experiments by emulation of an actual HMD were carried out in the laboratory by means of the set-up described in section 3. The results show a substantial improvement of up to 60% in the on target dwelling time and an improvement of up to 55% rms in the aiming accuracy.

2. Principle of Operation

The method for stabilization of a true helmet mounted-display image is described in Fig. 1. The target, T, is viewed through the semi-transparent visor from which the display is reflected to the pilot's eye. The hexagon, S represents a reticle projected to infinity. The acceleration, a, excites the biodynamic interferences in the human operator which is described by the biodynamic model Y_b . The biodynamic interference manifests itself as a vertical translatory head vibration accompanied by an angular head vibration of amplitude α , which causes S to shift with respect to T. The image of T on the retina remains fixed, and therefore sharp, because of the stabilizing mechanism of the Vestibulo-Ocular Reflex, (VOR). However, the symbol S, being fixed to the display, moves across the retina causing S to appear blurred. The head motion sensor, P, provides head position and orientation signals with respect to the cockpit. These signals

consist of the voluntary head motion, U_c , and the non-voluntary head motion, U_b , which, in the case described here, is the pitch head motion. The total head motion is defined as $U_t = U_c + U_b$. The adaptive algorithm provides estimated values \hat{U}_b of U_b and U_f of U_c which is derived from $U_f = U_t - \hat{U}_b$. In order to stabilize display elements against the additive vibration component, \hat{U}_b is fed into the display generator in opposite phase to the apparent shift of S, so that S appears to be stationary. This is shown in solid lines in Fig. 1.

In order to facilitate smooth head teleoperation, additional filtering must be provided to compensate for the non-additive non-voluntary head motion components N_{na} . Not being correlated with the cockpit motion, they cannot be suppressed by the adaptive algorithm. They give rise to additional relative shifts between the eye and the display and impair target acquisition and tracking. U_c is by nature of a much lower frequency than U_b . Therefore, U_f which is an estimate of U_c , is low-pass filtered to provide U_f^* in order to attenuate N_{na} . With the low-pass filtered signal U_f^* , two functions are performed as described in Fig. 1.

1. Subtraction of U_f^* from U_f . This is equivalent to its high-pass filtering.. The signal obtained is an estimate of N_{na} . It is added to \hat{U}_b and both are fed into the display generator in opposite phase with the head motion. The result is a less blurred sight, stabilized against the effects of U_b and N_{na} .
2. The low-pass filtered U_f is fed to the head slaved teleoperated device. The result is an improved correspondence between the motion of the slaved device and the voluntary head motion. In addition, the slaved device is not required to cope with high frequencies which may be outside its servo bandwidth.

The stabilization scheme is described in Fig. 1 for the elevation axis only. In reality, this scheme will be implemented both for the azimuth and elevation axes.

3. Experimental Investigation.

The experimental program had four goals of investigation:

1. Effects of vibration on head pointing accuracy.
2. The contribution of the adaptive filter to the pointing precision.
3. Effect of the low-pass filtering of U_f .
4. Relation between precision of tracking and pointing and the level of training.

The Experimental Set-up.

The experimental set-up consists of the following elements:

- 1) A six-degrees-of-freedom motion simulator.
- 2) A six-degree-of-freedom head motion (Polhemus) sensor.
- 3) Cabin mounted accelerometer.
- 4) Light weight helmet equipped with the head motion sensor and intercom.
- 5) Data acquisition and communication system.
- 6) Vax 750.
- 7) Motorola VME System 1131.
- 8) Image Technology Inc. Series 100TM Image Processor (FG-100)
- 9) Overhead TV Barco projector.

An overall view of the experimental set-up is shown in Fig. 2. The description of its principal subsystems is as follows:

- 1) The six-degrees-of-freedom-motion simulator:

The simulator was designed and developed at the Technion's Aerospace Flight Control laboratory. It has an electromechanical hexapod drive system using high-torque samarium-cobalt D.C. motors. It is digitally controlled, and it accepts commands both from inside the cabin and from external commands generated in the computer. Its bandwidth is about 15 Hz and its motion space is about 0.5 meters in translation and 30 deg in rotation. Its maximum acceleration is 1 g. The cabin construction is wood and plastic to avoid interference with the electromagnetic head motion sensor. For access, the the cabin hood is raised.

2) The Head motion Sensor:

The head motion sensor is a Polhemus "3space Tracker". It consists of three parts: The SEU (system electronics unit) to which two units are connected: The

source, or transmitter, which is mounted in the hood above the head, and the sensor, which is mounted on the helmet. The maximum sampling rate of the Polhemus is 60 Hz, but because of the limitations of the communication system the actual sampling rate was 37 Hz only. The static precision in translation is 2.5 millimeters rms and the angular precision is 0.5 deg rms. The resolution in translation is 0.75 millimeter and 0.1 deg in rotation. This level of precision can be obtained if the distance between the source and the sensor is between 10 and 70 centimeter. The measurements are transmitted to the computer serially via RS232 communication board.

In Fig. 3 the system block diagram is presented. The simulator motion is computed off-line by the Motorola computer. The motion time profile is read from a file and fed to the communication board into which the communication software has been loaded from the VAX 750. The simulator drive commands are fed to the motor amplifiers at a rate of 148 Hz. The vertical cabin acceleration, a , provided by the accelerometer is smoothed by a 15 Hz low-pass filter and is sampled by an A/D converter to provide a' which is fed into the Motorola computer. The effective sampling rate of the accelerometer and the Polhemus is 37 Hz. Depending on the filter configuration, the inputs into the reticle position shifting algorithm are:

- 1) U_t , or low-pass filtering of U_t in azimuth.
- 2) U_t , or U_f , or low-pass filtering of U_f in elevation.

The output signals of the reticle position shifting algorithm, and the target dynamics are fed into the display generator which drives the TV overhead projector. For each run the following data is recorded: U_t , \hat{U}_b , U_f , a' , and the adaptive algorithm convergence error, e^2 . Target position, x_t , y_t and reticle position, x_r , y_r , are processed after each run in order to enable immediate assessment of the performance of the subject.

Description of the Experiments:

In the experiments described here, an actual helmet sight was not yet

available. Therefore, the simulations were performed by emulating the tracking by means of a helmet sight as described in Fig. 5.

The reticle, represented by the rectangle subtending 0.58 deg high and 0.95 deg wide, and the target, represented by a cross, subtending 0.33 deg high and 0.54 deg wide, were projected on a screen placed 5 meters in front of the subject, with a display area of 14 deg high and 22 deg wide. The projected square emulated the collimated reticle of an actual helmet sight. The shifting of the square on the screen, in response to the angular head motion U_t , was therefore the emulation of a non-stabilized HMD sight, and it was implemented by means of the Polhemus signals. In order to implement the stabilization in an actual HMD, the square must be shifted in accordance with \hat{U}_b (Fig. 1). Thus, the emulation command for image stabilization is $U_t - \hat{U}_b = U_f$ (Fig. 5). In order to attenuate the effect of N_{na} , U_f is high-pass filtered and added to the stabilizing signal \hat{U}_b when using an actual HMS. This is equivalent to the low-pass filtering of U_f in the emulation. The task of the subjects was to align the reticle with the target so that it appeared to be at its center.

In the experiments the adaptive filter was presently implemented in the elevation axis only because of the current computational limitations.

Four experiments were performed:

- 1) Stationary Target, Cabin motion: Vertical, sinusoidal:

Frequency: 5 Hz.

Acceleration: 0.069 g rms.

Number of Subjects: 4.

- 2) Moving target, cabin motion: Vertical, sinusoidal,

Frequency: 5 Hz.

Acceleration: 0.069 g rms.

Target motion: Gaussian zero-mean white noise filtered by a second order low-pass filter (LPF) with 0.03Hz frequency and damping ratio of 0.5. Altogether there were three different target motions with amplitudes ranging 2.8 -2.9 deg rms.

Number of Subjects: 4.

- 3) Stationary target, cabin motion sinusoidal and random:

Vertical, sinusoidal at 4 Hz and a random component derived from zero-mean Gaussian white noise filtered by a second order LPF with damping ratio of 0.5 and a cut-off frequency of 3 Hz which represents high frequency turbulence.

Acceleration: 0.035 g rms.

Number of subjects: 3.

- 4) Stationary target, cabin motion random, vertical and pitch:

The random signal was obtained from zero-mean Gaussian white noise filtered by a second order LPF with a damping ratio of 0.5 and a cut-off frequency of 0.5 Hz which represents typical atmospheric turbulence.

Acceleration: 0.032g rms.

Number of subjects: 2.

Experiments 1 and 2 represent helicopter flight without turbulence. The periodic component is caused by the rotor. Experiment 3 represents helicopter flight at low altitude where high frequency turbulence can be encountered. Experiment 4 represents ordinary low frequency turbulence in the absence of rotor induced vibration.

The choice of the simulator motion and target motion was done in consultation with fighter and helicopter pilots who also actively participated in the motion tuning.

In each of the four experiments the following helmet sight operation modes were tested:

- 1) Stationary cabin, (No Vibration).
- 2) Vibrating cabin, unstabilized sight (No Filtering).
- 3) Vibrating cabin, stabilized sight by an adaptive filter only (AF)
- 4) Vibrating cabin, stabilized sight by low-pass filtering only (LPF).
- 5) Vibrating cabin, stabilized sight by adaptive and low-pass filtering (AF +LPF).

Each run lasted 90 seconds. The first 15 seconds were assigned to allow the

subject to settle in his posture, leaning on the back support of the seat. The next 15 seconds were assigned for the final settling of the adaptive filter. Following this 15 second time period the reticle would appear, initially centered over the target which was, in turn, centered in the display field. During the remaining 60 seconds, the actual tracking tasks were performed. The results were recorded 5 seconds after the beginning of the tracking phase.

Because of computational limitations in real time, \hat{U}_b and U_f were estimated for the elevation axis only. the LPF was implemented in both axes.

The Subjects and Their Training:

Four subjects participated in the pointing and tracking experiments, (GS, OC, MI, OL). All of them students in the Technion Department of Aerospace Engineering. They were all paid a basic fee and additional premiums for good performance to increase motivation. OL is female and wearing soft contact lenses. GS wore spectacles. MI has pilot experience in light aircraft. Table 1 describes their physiques.

Table No. 1: Data on Subjects' Physiques.

Subject	Age [years]	Weight [Kg]	Height [Cm]	W/H Ratio. $W/H = \frac{\text{Weight [Kg]}}{\text{Height [Cm]} - 100}$
GS	22	60	177	0.77
MI	25	70	170	1.00
OC	26	90	185	1.05
OL	24	50	168	0.73

Before starting the actual tests, the subjects underwent an initial training period in the simulator of about six hours each, in the course of which, about 15 runs for each configuration were executed. On the average, 12 runs were executed per hour. After each subject reached a stable level of performance, 10 additional runs were performed for each configuration. These were used in the actual data

recording and processing.

The Adaptive and Low-Pass Filters:

A description of the adaptive filter can be found in the appendix. The filter length was determined in accordance with the model given in and ⁷ and was set to $T=0.81$ sec. Since the sampling rate, determined by the Polhemus and the communication system is 37 Hz, the sampling rate was chosen at $\Delta T = 2\text{msec}$ so that the number of weights in the filter is $N = 30$. The gain parameter was set to $f = 9$ and the parameters of the variable gain were chosen at $c_t = 0.001$ and $c_s = 0.0011$; The threshold for freezing the weights was set to $e_0 = 1$. The break point of the high-pass filter for U_t was set to 15 rad/sec since the dominant frequency of the non-voluntary head motion was in the region of 4 - 5 Hz. On the average the adaptive filter, as implemented in these experiments, converges in 2.5-3 seconds. The adaptive filter algorithm also incorporates cut-off mechanism as explained in the appendix. The cut-off frequency of the LPF for N_{na} was set to 2 rad/sec. This choice was a good compromise between the need to attenuate these noise components and avoiding excessive phase lag in the motion of the reticle. The low-pass filter was disconnected when the head angular rate exceeded 30 deg/sec and was reconnected when it decreased to less than 30 deg/sec.

Data Processing:

Since \hat{U}_b and U_f were estimated in the elevation axis only, data were processed accordingly and they are divided into two parts:

- 1) Evaluation of the performance of the AF: Analysis of the estimated signals \hat{U}_b and U_f , the vector of weights \underline{w} , and the convergence of the squared adaptation error e^2 .
- 2) Evaluation of the performance of the human operator in head pointing and tracking tasks. In particular, two parameters were observed:
 - a. The dwelling time of the reticle on the target: The percent iteration of the total in a run, within which the distance between the respective centers of the target and the reticle was smaller than half the height of the reticle.
 - b. The rms tracking error: The rms values of the above distance between reticle

and target centers was determined.

The performance of each subject was evaluated for all the configurations, and for each of the three experiments, this by averaging the results of 10 runs, each consisting of over 2000 data points. Also, the results of all the subjects for all the configurations were averaged for each of the three experiments.

Results of the Experiments

Table 2 describes the results obtained in experiments 1 - 3.

Table 3 describes the results of experiment 4.

Experiment No.1: Stationary Target:

From Table 2 one can see that without vibration the reticle was 'on-target' on the average, for more than 99% of the total time and that the rms pointing error was 0.08 deg. Vibration without filtering caused a decrease of percent dwelling time to 69.2% and an increase in pointing error of 0.18 deg rms. With the AF, the percentage dwelling time increased by 11.8% and a decrease in tracking error of 10.1% rms was recorded. With the AF + LPF configuration, the percent dwelling time increased by 36% and the pointing error decreased by 49%. No significant differences were found between the respective performance with the LPF alone and the AF + LPF configurations. The reason for this is that the AF was originally designed to suppress the additive biodynamic interference only, which, as stated in section 2, is accompanied by non-additive remnant noise N_{na} with which the AF cannot cope but the LPF can. The performance of the subjects with the LPF were only slightly worse than their performance without vibration. Subject OC performed best of all the subjects with the AF only probably because of his heavy physique ($W/H = 1.05$), which probably gave rise only to small values of the non-additive component N_{na} . The relative improvement in his performance due to the LPF was smaller than for the other subjects. Subject MI did not do well with the AF alone. All the other subjects stated that the task was considerably easier with the AF as compared to no filtering at all. All the subjects stated that the inclusion of the LPF alleviated the pointing task substantially. Figures 6(a) to 6(c) which describe angular head motion along with their respective filtered

outputs, demonstrate the effectiveness of the algorithm in suppressing U_b and the effectiveness of the LPF in filtering N_{na} .

Experiment No.2: Moving Target:

From Table 2 one can see, that on the average the percent dwelling time without vibration was 87.2% and the tracking error was 0.166 deg rms. Vibration caused a decrease of 25% in percent dwelling time and an average increase of 75%rms in tracking error. The inclusion of the adaptive filter caused an increase of 13.6% in percent dwelling time and a decrease of 16.7% in rms tracking error. The use of the LPF, with or without the AF, caused an increase of 31% in percent dwelling time and a decrease of 35% in rms tracking error, in comparison with no filtering. The influence of the individual physiques of the subjects was again noticed. Subject OL and GS who have light physiques experienced substantial difficulties under vibration without filtering. The AF, in their case, had only a limited effect apparently, because with a moving target, the non-additive component N_{na} increased substantially. For subject OC, on the other hand, the LPF had only a slight effect on his level of performance. The LPF, enabled all the subjects to reach almost the same level of performance.

Figures 7(a) to 7(c) demonstrate the effectiveness of the AF to suppress U_b , and the effectiveness of the LPF to filter N_{na} from U_f . Observation of e^2 , the squared adaptation error, discloses that the presence of N_{na} persistently causes small estimation errors, which do not exist in viewing task where N_{na} is much smaller⁷.

Experiment No. 3: Stationary Target, High Frequency Turbulence:

This test demonstrates that N_{na} with random vibration is larger than with sinusoidal vibration. From Table 2 one can see that the performance, without any filtering, was significantly worse in experiment No. 3 than in the other tests. It is also noticeable that the AF in this case is less effective in improving tracking precision because of the relatively large N_{na} . On the other hand, an average increase of 60% in percent dwelling time and a decrease of 55% in rms tracking error is achieved by the inclusion of the LPF. This is the largest

relative improvement of all the tests performed which underlines the effectiveness of the LPF in filtering N_{na} . Figures 8(a) to 8(c) which describe U_f , U_c and U_b after the LPF, again demonstrate the effectiveness of the AF to separate U_b from U_c , and the effectiveness of the LPF in filtering N_{na} .

Experiment No. 4: Stationary Target, Low Frequency Turbulence:

Table No. 3 shows the results of the subjects' performance after having gained tracking experience of tens of hours in previous tasks. It can be seen that after two runs the difference of performance between LPF and LPF + AF was 5%. After an interval of 3 days, there was still a difference of 6% between these two configurations. However, after some additional training, the difference decreased to insignificant values. Throughout the extent of the learning process it was found that the LPF yields performance levels which are very close to the performance without vibration. A possible explanation is, that initially, the subject requires the filtering of both the additive and non-additive components of interference. In the process of learning, the subject learns to compensate the additive component by adjusting his posture and his muscle tone, and eventually he does not need the assistance of the adaptive filter. The improvement in percent dwelling time from the initial value of 92% to the final value of 96% with the AF+LPF configuration may be explained by the pilot's ability to overcome the time lag introduced by the LPF. At vibration frequencies below 0.5 Hz no deterioration in tracking performance was noted, apparently, because this frequency is within the bandwidth of the neuromuscular reflex.

Table No. 2: Average Results of Teleoperation Experiments 1-3

Exp. No.	Config.	Dwelling Time [%]	Dwelling Time Improvement [%] Compared With No Filtering	Tracking Error RMS [DEG]	Tracking Error Improvement [%]
1	Stationary	99.2		0.082	
	No Filters	69.2		0.258	
	AF	77.4	11.8	0.232	10.1
	LPF	93.2	34.7	0.135	47.7
	AF+LPF	94.1	36.0	0.132	48.8
2	Stationary	87.2		0.166	
	No Filters	63.1		0.288	
	AF	71.7	13.6	0.240	16.7
	LPF	84.1	33.3	0.179	37.8
	AF+LPF	82.4	30.6	0.187	35.1
3	Stationary	99.2		0.082	
	No Filters	55.8		0.357	
	AF	60.4	8.2	0.303	15.1
	LPF	87.0	55.9	0.165	53.8
	AF+LPF	89.0	59.5	0.161	54.9

Table No3: Results of Learning Experiments:

Configuration	Dwelling Time [%]	Tracking Error RMS [DEG]
Average after two runs:		
No Filtering	65.9	0.280
AF	73.9	0.230
LPF	87.4	0.174
AF+LPF	92.1	0.138
After three days of a different task:		
LPF	91.4	0.142
AF	97.3	0.120
The next day:		
No Filtering	69.5	0.260
AF	74.0	0.226
LPF	96.4	0.128
AF+LPF	96.8	0.115

4. Summary of Experimental Results

Table 4 compares the performance improvement using the AF only.

Table No. 4: Dwelling Time Improvement [%] With Adaptive Filter

Experiment No.	Motion Description	Dwelling Time Improvement [%] AF Relative to No Filtering
1	Deterministic (Heave)	11.8
2	Deterministic + Random (Heave)	8.2
3	Random (Heave)	6.5
4	Random (Heave + Pitch)	3.0

From Table No. 4 one learns that the larger the random component in the vibration, the smaller is the contribution of the AF. The non-additive component is the dominant interference which the AF cannot handle.

As a rule, the finding is that in pointing and tracking tasks, the dominant interference is non-additive which is more readily filtered by the LPF. The experiments indicate that, at least with the time constants of 0.5 seconds, the subjects learned to compensate for the additional phase lag introduced by the LPF. As a rule all the subjects reached similar levels of performance, and eventually, after sufficient training, and with the adaptive and low-pass filtering configuration, it closely approached the tracking error level without vibration.

5. Acknowledgements

This work has been supported in part by the Human Factors Division, NASA Ames Center and by the USAF Aerospace Medical Research Laboratory, WPAFB, under grants NAWG 1128 and AFOSR88 0298, respectively.

6. References

1. Levison, W.H. Baron, S. and Junker, A.M., "Modeling the Effects of Environmental Factors on Human Control and Information Processing", Wright-Patterson Air Force Base, Ohio, AMRL-76-74, August 1976.
2. Jex, H.R., "Problems in Modeling Man Machine Control Behavior in Biodynamic Environments", *Proc. 7th Annual Conf. on Manual Control*, NASA SP-281, 1971.
3. Wells, M.J. and Griffin, M.J., "Benefits of Helmet Mounted Display Image Stabilization Under Whole-Body Vibration", *Aviation, Space and Environmental Medicine*, January 1984.
4. Lewis, C.H. and Griffin, M.J., "Predicting the Effects of Vertical Vibration Frequency, Combination of Frequencies and Viewing Distance on the Reading of Numeric Displays". *Journal of Sound and Vibration*, 1980.
5. Wells, M.J. and Griffin, M.J., "Performance with Helmet Mounted Sights", ISVR Technical Report 152, University of Southampton, September 1987.
6. Wells, M.J. and Griffin, M.J., "Tracking with the Head During Whole-Body Vibration", *Training, Human Decision Making and Control*, J. Patrick and K.D. Duncan (Eds.), Elsevier Science Publishers, B.V. (North-Holland), 1988.
7. Lifshitz, S. and Merhav, S.J., "Adaptive Suppression of Biodynamic Interference in Helmet Mounted Displays and Head Teleoperation", accepted for publication, *AIAA J. of Guidance Navigation and Control*.
8. Nicholson, R.M., "The Feasibility of a Helmet Mounted Sight as a Control Device", *Human Factors* 8(5), 417-425, 1966.
9. Grossman, J.D., "Flight Evaluation of Pilot Sighting Accuracy Using a Helmet Mounted Sight". Naval Weapons Center, China Lake, California, Report No. NWCTP 5638, 1974.
10. Simpson, T., Wells, M.J., Lewis, C.H. and Griffin, M.J., 1983: Unpublished research data.
11. Verona, R.W., "Head Aiming/Tracking Accuracy in a Helicopter Environment". Presented at the Aerospace Medical Association Conference, May 1978.

12. Tatham, N.O., "The Effect of Turbulence on Helmet Mounted Sight Aiming Accuracies", AGARD, CP-267, March 1980.
13. Widrow, B. and McCool, J.M., "A Comparison of Adaptive Algorithms Based on the Method of Steepest Descent and Random Search", *IEEE Trans. on Antennas and Propagation*, Vol. AP-24, No. 5, Sept. 1976.
14. Merhav, S.J., "Adaptive Suppression of Biodynamic Interference in Helmet Mounted and Head Down Displays". *AIAA Guidance, Navigation and Control Conference*, Minneapolis, Minnesota, August 1988.
15. Haykin, S., "Adaptive Filtering Theory", Book, Prentice-Hall Information Systems Science Series, 1986.
16. Velger, M., Grunwald, A. and Merhav, S., "Suppression of Biodynamic Disturbances and Pilot-Induced Oscillations by Adaptive Filtering", *AIAA J. of Guidance, Control and Dynamics*, July-August 1984, pp. 401-409.
17. Velger, M., Grunwald, A. and Merhav, S., "Adaptive Filtering of Biodynamic Stick Feedthrough in Manipulation Tasks on Board Moving Platforms", *AIAA J. of Guidance, Control and Dynamics*, Vol. 11, No. 2, March-April 1988.
18. Honig, M.L., Messerschmitt, D.G., "Adaptive Filters, Structures, Algorithms and Applications", Book, Kluwer Academic Publishers, 1984.

Appendix

The Adaptive Filter.

The adaptive filter is based on the well known Least Mean Square (LMS) algorithm widely used in adaptive noise cancellation applications. It is an extension of the classical LMS described in Widrow and McCool¹³. Its main advantages are small computational load, global stability and robustness. The extended LMS used in this paper has the additional advantages of rapid adaptation to variations in model parameters and the precise estimation of the relatively small disturbance U_b in the presence of large voluntary head motion U_c . This issue is addressed in Merhav¹⁴. Other algorithms such as Root Least Square (RLS) and Lattice filters, Haykin¹⁵, were considered because of their superior convergence in terms of the number of iterations. However, in view of their larger computational complexity, longer iteration times and lower robustness where rapid variations in model parameters are involved, they were not adopted in the present study. In view of these considerations and the successful implementation of the basic LMS in suppressing biodynamic disturbances in manual control, Velger and Merhav^{16,17}, the extended LMS was used in the work described here.

The extended LMS filter

Figure A.1 describes the basic LMS filter in conjunction with the variables and parameters described in Sec 2 above and in its role of noise suppression. The error e_j which drives the algorithm is given by

$$e_j = U_{c_j} + U_{b_j} - \hat{U}_{b_j} = U_{c_j} - \tilde{U}_{b_j} \quad (A-1)$$

j is the index of the sampled process. The estimation error \tilde{U}_b is given by

$$\tilde{U}_{b_j} = U_{b_j} - \hat{U}_{b_j} \quad (A-2)$$

U_c adds to e and upsets the proper convergence of the algorithm. Therefore, in order to assure $\hat{U}_b \rightarrow U_b$, it is necessary to fulfill the condition that $U_c \ll U_b$. Assuming that the parameter variations of the human biodynamic model are relatively slow and small, \hat{U}_b converges to U_b with satisfactory precision. The filtered signal U_f therefore is given by:

$$U_{f_j} = U_{c_j} + U_{b_j} = U_{c_j} + \tilde{U}_{b_j} \approx U_{c_j} \quad (A-3)$$

Equation (A-3) indicates that the biodynamic interference due to a is essentially canceled. In reality, the condition $U_c \ll U_b$ is not fulfilled. U_c can be in the order of 90 deg or more, while U_b is normally in the order of 1 deg. The variations in the parameters of the human biodynamic model are not necessarily slow. They may be rather rapid as a result of sudden changes in posture or muscle tone. Therefore, the basic filter, as shown in Fig. A.1, does not meet all the requirements. The extended LMS filter, which can estimate both U_b and U_c , is shown in Fig. A.2. A high-pass filter, for example of the type $s/(s+k)$, is inserted both in the Y_b and the AF path in order to maintain proper phase balance. The error e now is

$$e_j = \frac{s}{s+k} \left(U_{t_j} - \hat{U}_{b_j} \right) = \frac{s}{s+k} \left(U_{c_j} - \tilde{U}_{b_j} \right) \quad (A-4)$$

Thus, with the high-pass filters, e is affected by changes in U_c and not by U_b itself. Consequently, the estimated gradient is given by

$$\hat{\nabla}_j = 2e_j \frac{\partial e_j}{\partial \underline{w}_j} = -2e_j \left\{ \frac{s}{s+k} \underline{x}_j \right\} \quad (A-5)$$

And the extended LMS algorithm takes the form

$$\underline{w}_{j+1} = \underline{w}_j + 2\mu_j e_j \left\{ \frac{s}{s+k} \underline{x}_j \right\} \quad (A-6)$$

Where \underline{x}_j represents the accelerations a_j , μ_j is the gain and \underline{w} is the weight vector. In the actual implementation, a is high-pass filtered in order to reduce the effects of sensor bias and gravity.

The estimate of the nonvoluntary head motion \hat{U}_b is

$$\hat{U}_{b_j} = \underline{w}_j^T \underline{x}_j \quad (A-7)$$

and the estimate of the voluntary head motion U_f is

$$U_{f_j} = U_{t_j} - \hat{U}_{b_j} = U_{c_j} + \tilde{U}_{b_j} \quad (A-8)$$

In order to assure that the convergence rate of the algorithm is independent of the input intensity \underline{x} , μ_j is chosen such that

$$\mu_j = \frac{1}{f \text{tr}(\underline{R}_j)} \quad (A-9)$$

where f is a constant coefficient $f > 1$ and \underline{R} is the covariance matrix of the

input \underline{x} . This choice of μ_j yields the Normalized LMS (NLMS). The spread of the eigenvalues of R is reduced by the square root of the spread as compared to the basic LMS algorithm. The rate of convergence and its sensitivity to eigenvalue spread are substantially reduced, Honig and Messerschmitt¹⁸.

Rapid adaptation requires a large μ . In accordance with Eq. (A-9) this implies a small f . The smaller f , the larger the misadjustment noise in the estimated weight vector \underline{w} , Widrow and McCool¹³. On the other hand, the smaller μ , the slower the adaptation rate. A remedy to this conflict is to implement an error-dependent $\mu = \mu(e)$, where $\mu(e)$ is a monotonic function in e independent of $\text{sgn}(e)$. Thus, if e , for example, increases as a result of a change in Y_p , μ is large and the adaptation is rapid. Yet, once convergence proceeds, μ becomes small, and the misadjustment noise becomes small. The implementation of μ is as follows: We choose μ_0 in accordance with the stability criterion of the algorithm, Widrow and McCool¹³, namely

$$\mu_0 = \frac{1}{f \text{tr}(R_j)} \quad (\text{A-10})$$

We define:

$$\underline{e}_j \triangleq [e_j, e_{j-1}, \dots, e_{j(N'-1)}]^T \quad (\text{A-11})$$

where $N' > N$

let

$$\underline{e}_j^2 \triangleq \underline{e}_j \underline{e}_j^T = \sum_{i=j-(N'-1)}^j e_i^2 \quad (\text{A-12})$$

$$\epsilon_j \triangleq \left[\frac{\underline{e}_j^2}{\text{tr}(R_j)} \right]^{1/2} \quad (\text{A-13})$$

a possible method to implement $\mu(e)$ is: We define threshold and saturation values ϵ_t and ϵ_s and we prescribe $\mu = \mu(e)$ in accordance with Eq. (A-14):

$$\mu_j(e) = \begin{cases} 0 & 0 \leq \epsilon_j < \epsilon_t \\ \frac{\epsilon_j - \epsilon_t}{\epsilon_s - \epsilon_t} \mu_0 & \epsilon_t \leq \epsilon_j < \epsilon_s \\ \mu_0 & \epsilon_s \leq \epsilon_j \end{cases} \quad (\text{A-14})$$

However, large angular head motion, in spite of the high-pass filter $s/(s+k)$, will still cause large transients in e and perturbations in \underline{w} . In order to overcome this problem, we set $\mu_j(\varepsilon)=0$ whenever the error e exceeds a given threshold e_0 . We divide e into two components, namely e_c resulting from large head motion, and e_b , resulting from the nonvoluntary head motion. Thus,

$$e_j = e_{c_j} + e_{b_j} \quad (A-15)$$

Whenever $|e_j| > e_0$, $\mu_j(\varepsilon) = 0$ and \underline{w} is frozen. e_0 is so chosen that $\text{Prob}\{e_j \geq e_0\} \rightarrow 1$ whenever the variations in U_c are large. When the variations in U_c are small, the threshold e_0 must fulfill the condition $\text{Prob}\{e_{b_j} \geq e_0\} \rightarrow 1$. The advantage of freezing the weights is, that after a large change in U_c , only a short time is needed to re-establish a good estimate of U_b . The disadvantage is that during the freezing intervals, parameter tracking is inhibited.

Bias and g components in the accelerometers degrade the convergence of the algorithm and cause errors in the estimate of U_b . This can be overcome by additional high-pass filtering of the accelerometer readings.

Figure Captions

Fig. 1. HMD stabilization - principle of operation.

Fig. 2. The experimental set-up.

Fig. 3. The experimental set-up block diagram.

Fig. 4. Head teleoperation task.

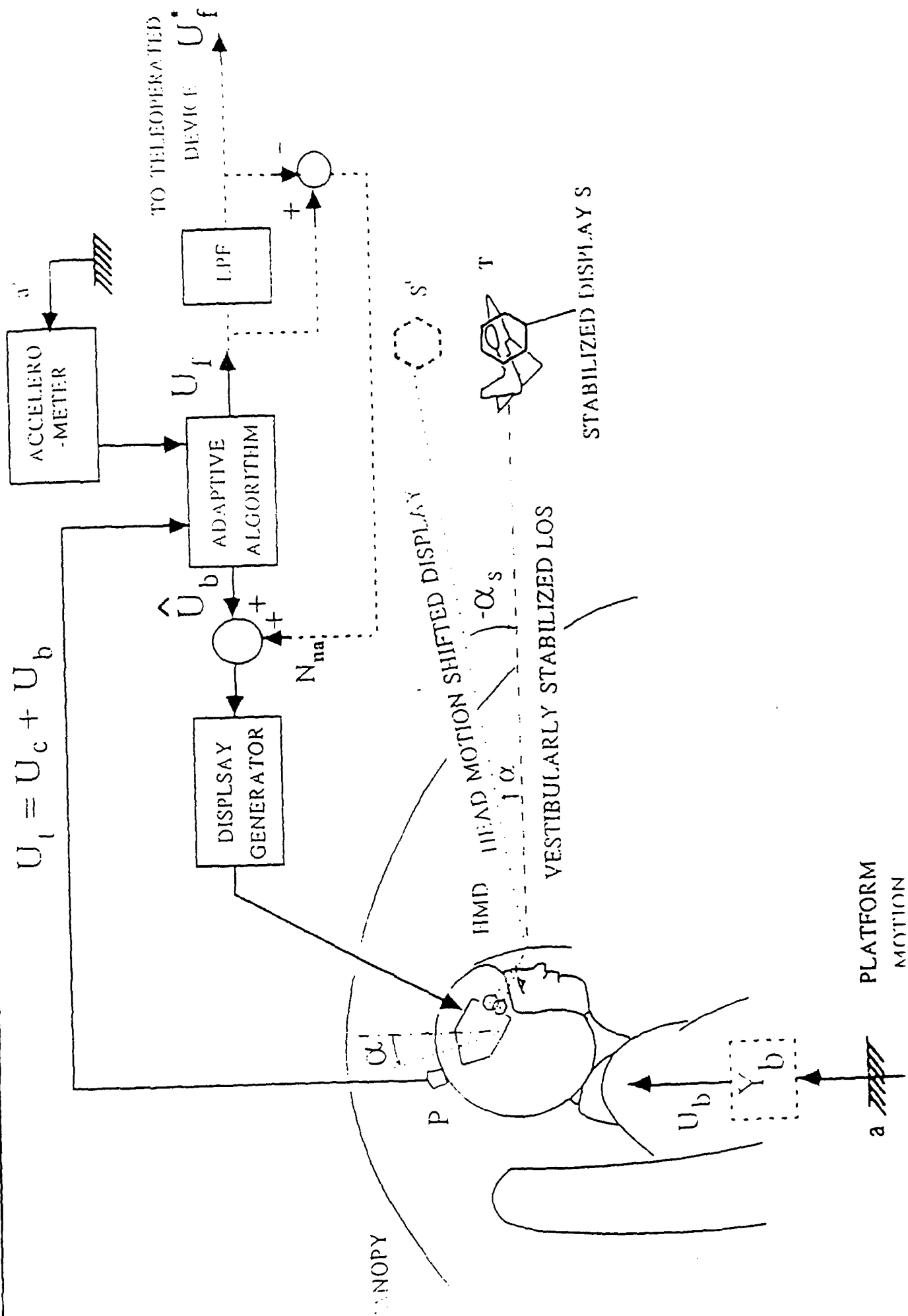
Fig. 5. (a,b,c). A section of the time history of a) total head motion U_t ; b) estimated voluntary head motion U_f ; c) LPF of U_f , for the example with a stationary target (experiment no. 1).

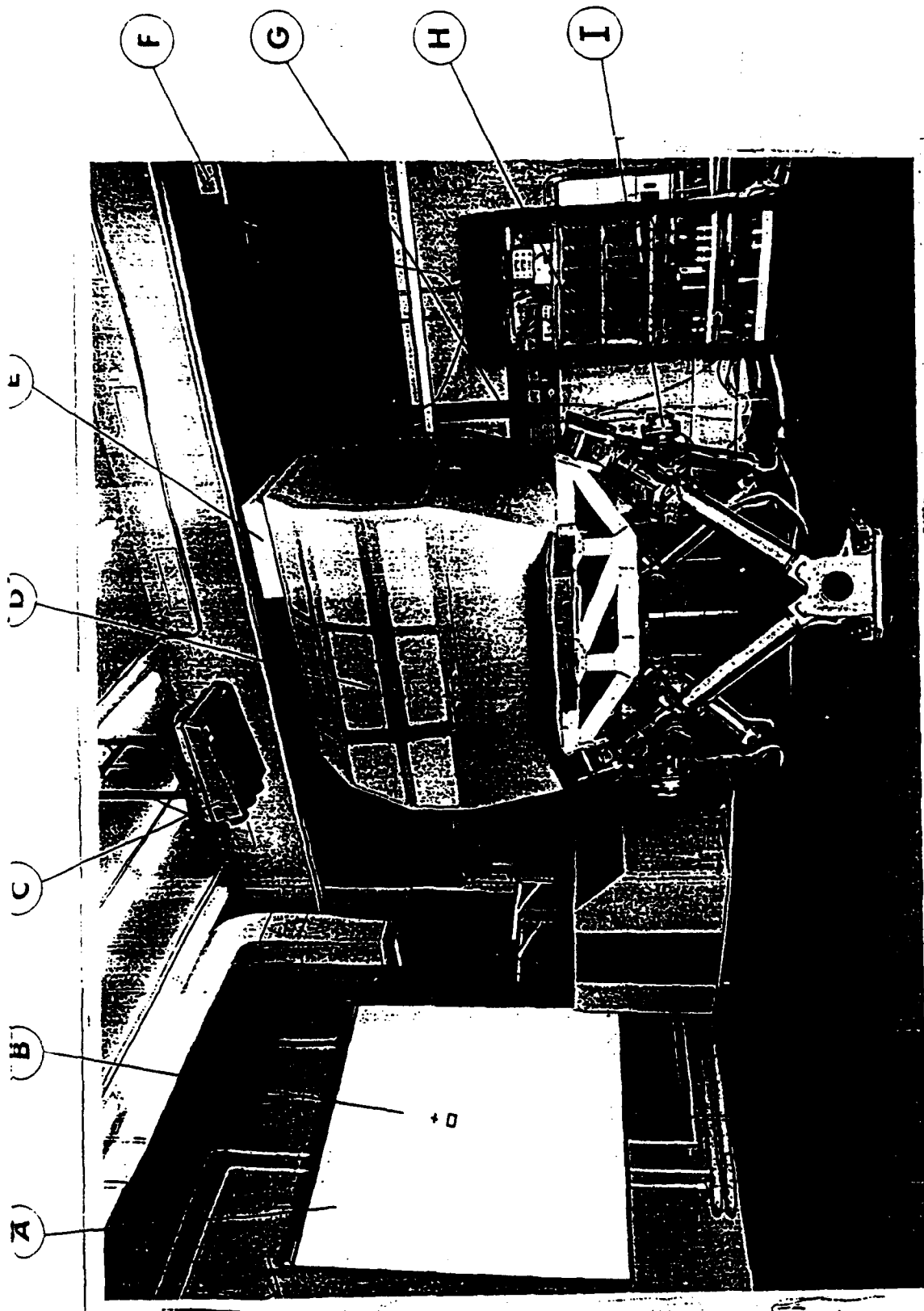
Fig. 6. (a,b,c). A section of the time history of a) total head motion U_t ; b) estimated voluntary head motion U_f ; and c) LPF of U_f , for the example with a moving target (experiment no. 2)

Fig. 7. (a,b,c). A section of the time history of a) total head motion U_t ; b) estimated voluntary head motion U_f ; c) LPF of U_f , for the example with a moving target (experiment no. 3)

Fig. A.1 Basic LMS algorithm for suppression of biodynamic interference in HMD and head teleoperation.

Fig. A.2 Extended LMS algorithm for suppression of biodynamic interference in HMD and head teleoperation.





- | | |
|--------------------------|--------------------------------------|
| A - screen | F - Polhemus SEU |
| B - display | G - accelerometer |
| C - overhead projector | H - power amplifier unit |
| D - cabin | I - electro-mechanical motion system |
| E - Polhemus transmitter | |

Figure 2: The experimental setup.

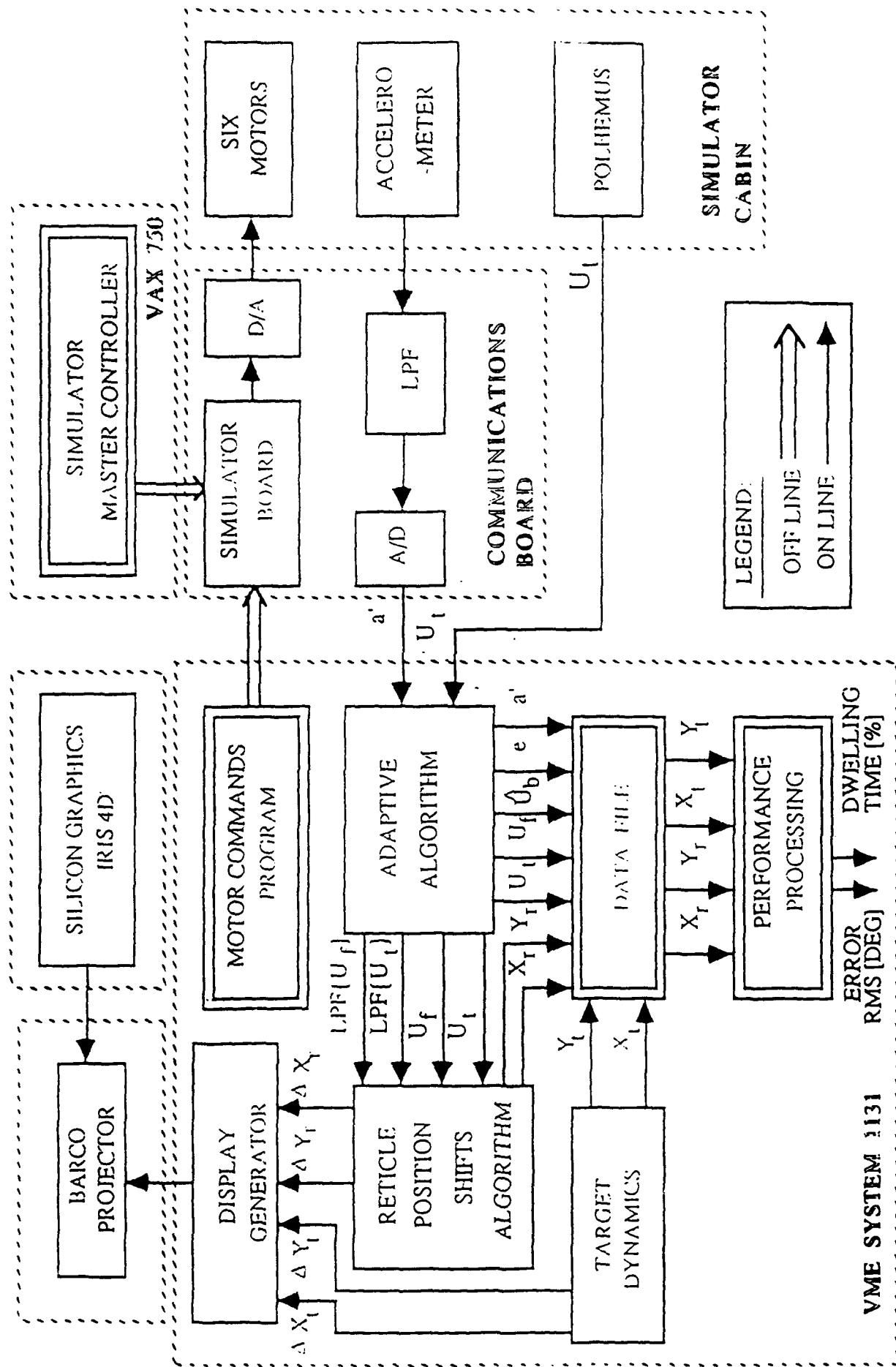


Figure 3. The experimental set-up block diagram.

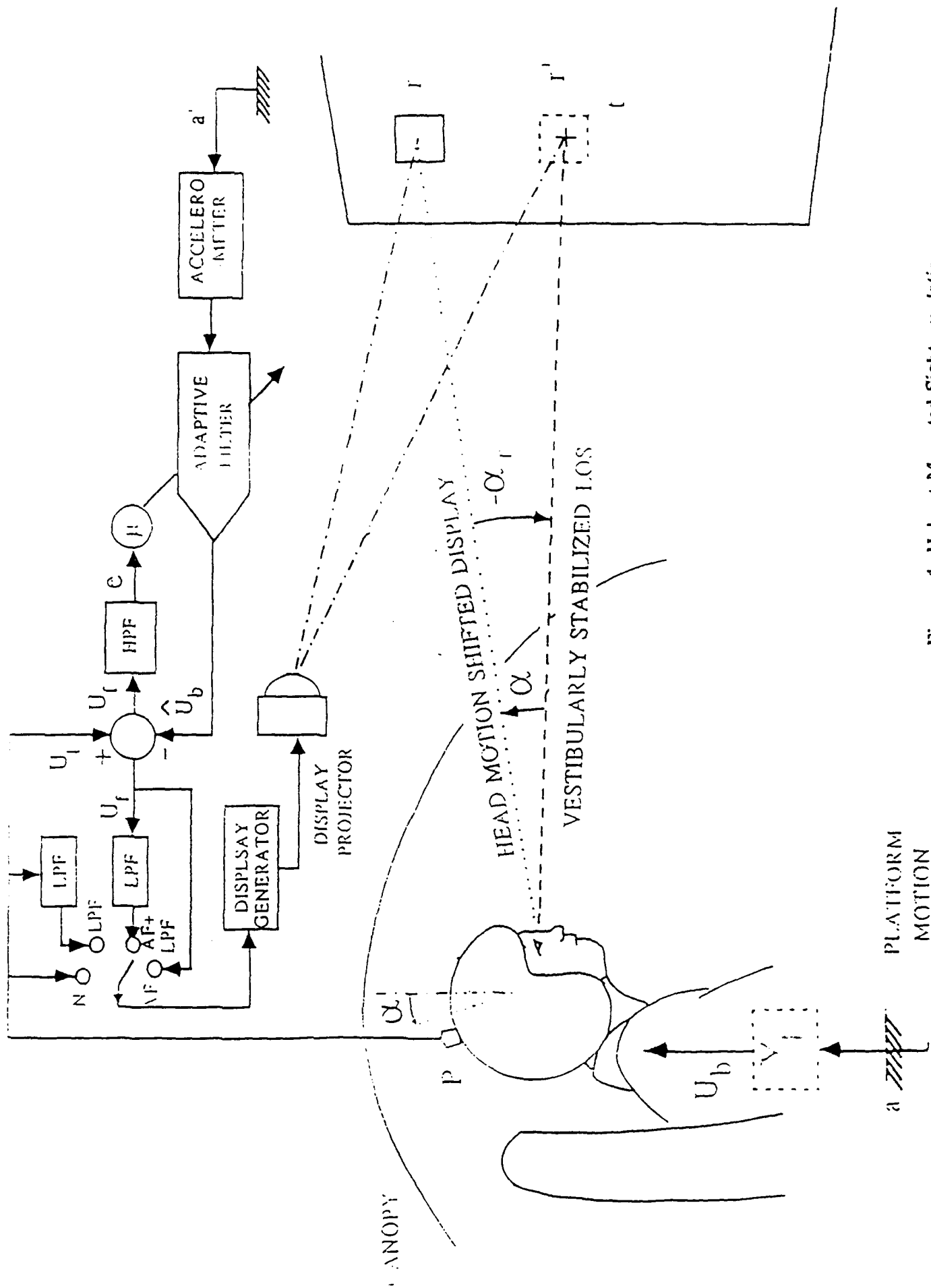


Figure 4. Helmet Mounted Sight emulation.

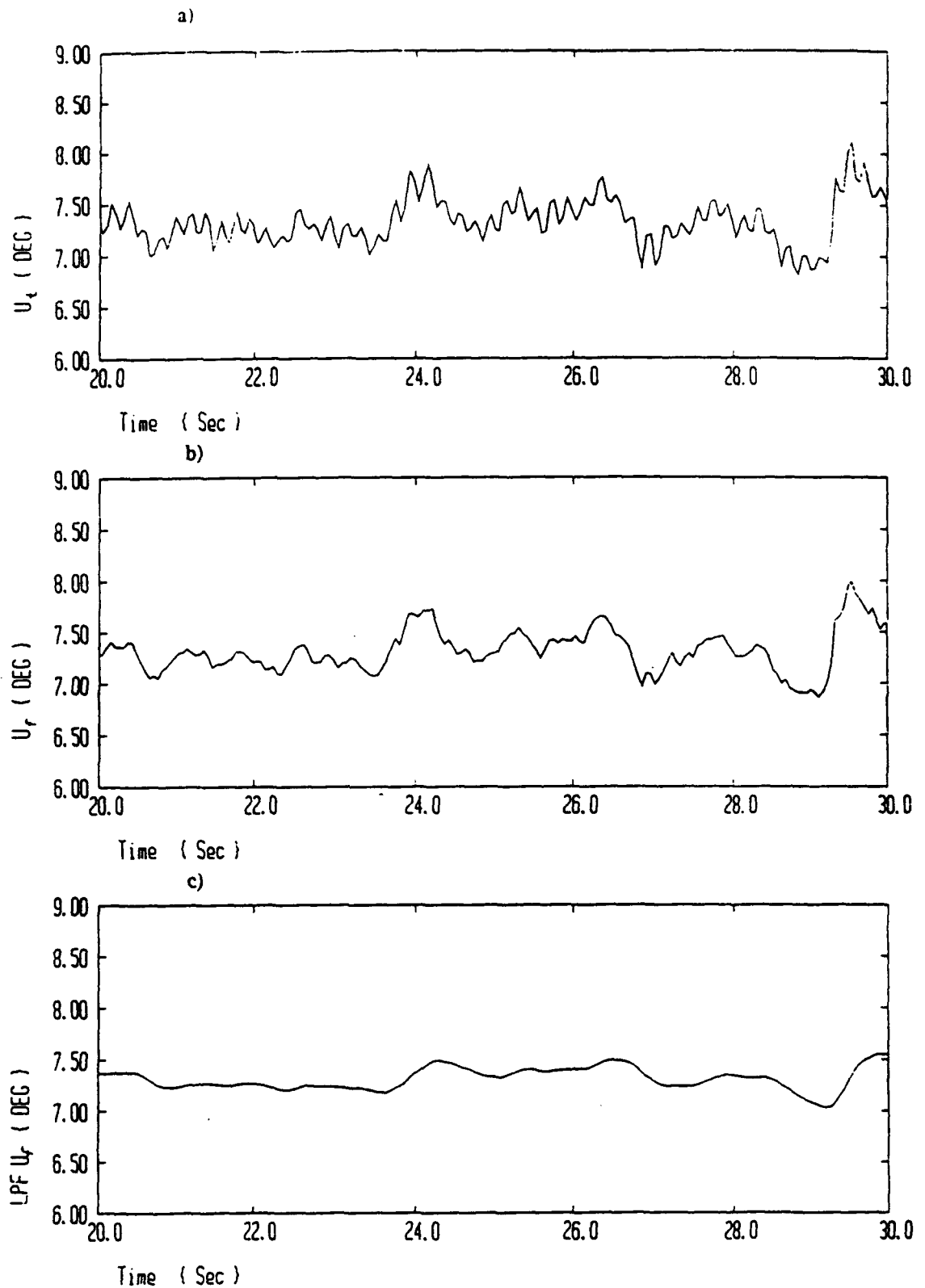


Fig. 5. (a,b,c). A section of the time history of a) total head motion U_t ; b) estimated voluntary head motion U_r ; and c) LPF of U_r , for the example with a stationary target (experiment no. 1).

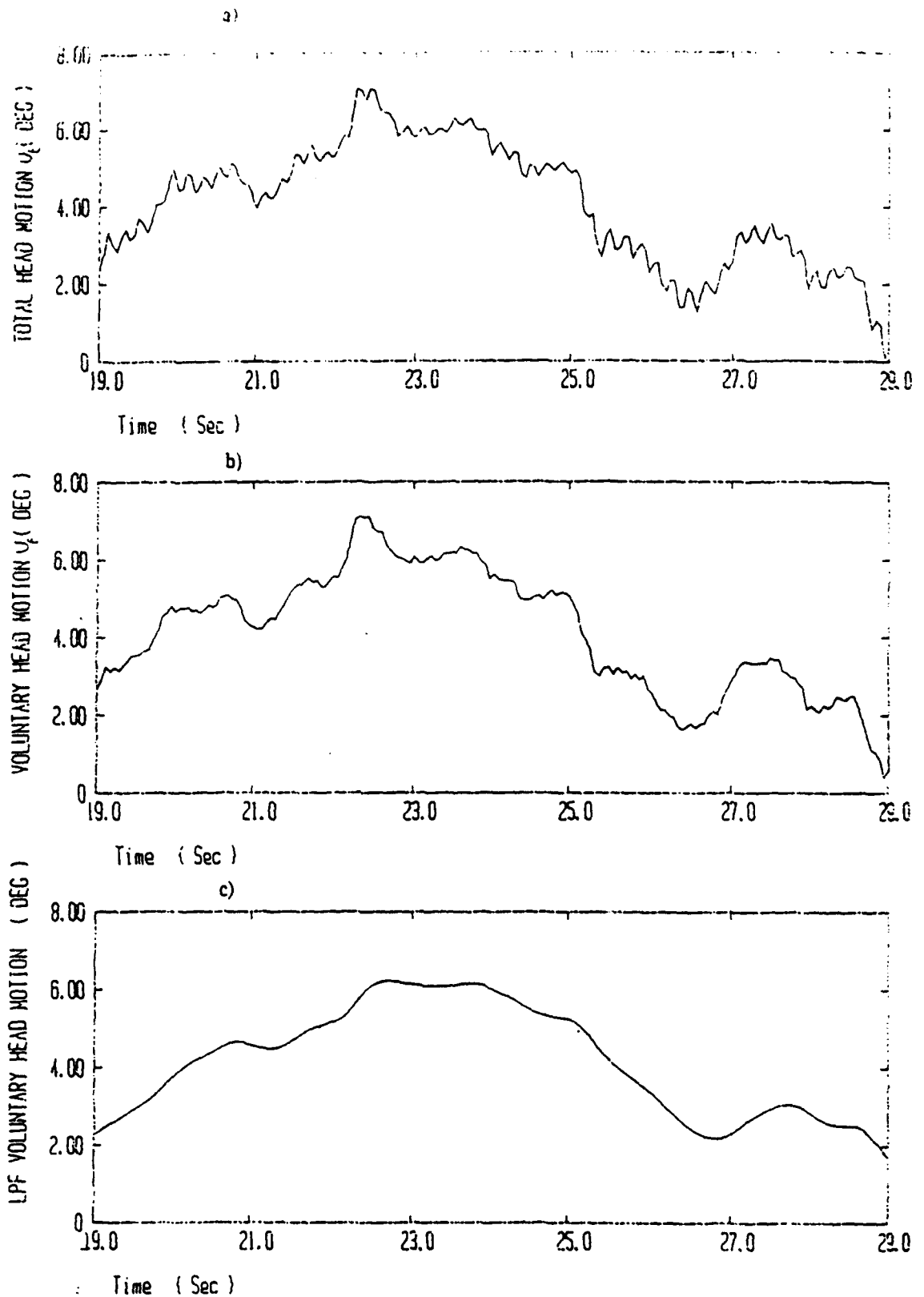


Fig. 6. (a,b,c). A section of the time history of a) total head motion U_t ; b) estimated voluntary head motion U_v ; and c) LPF of U_v , for the example with a moving target (experiment no. 2).

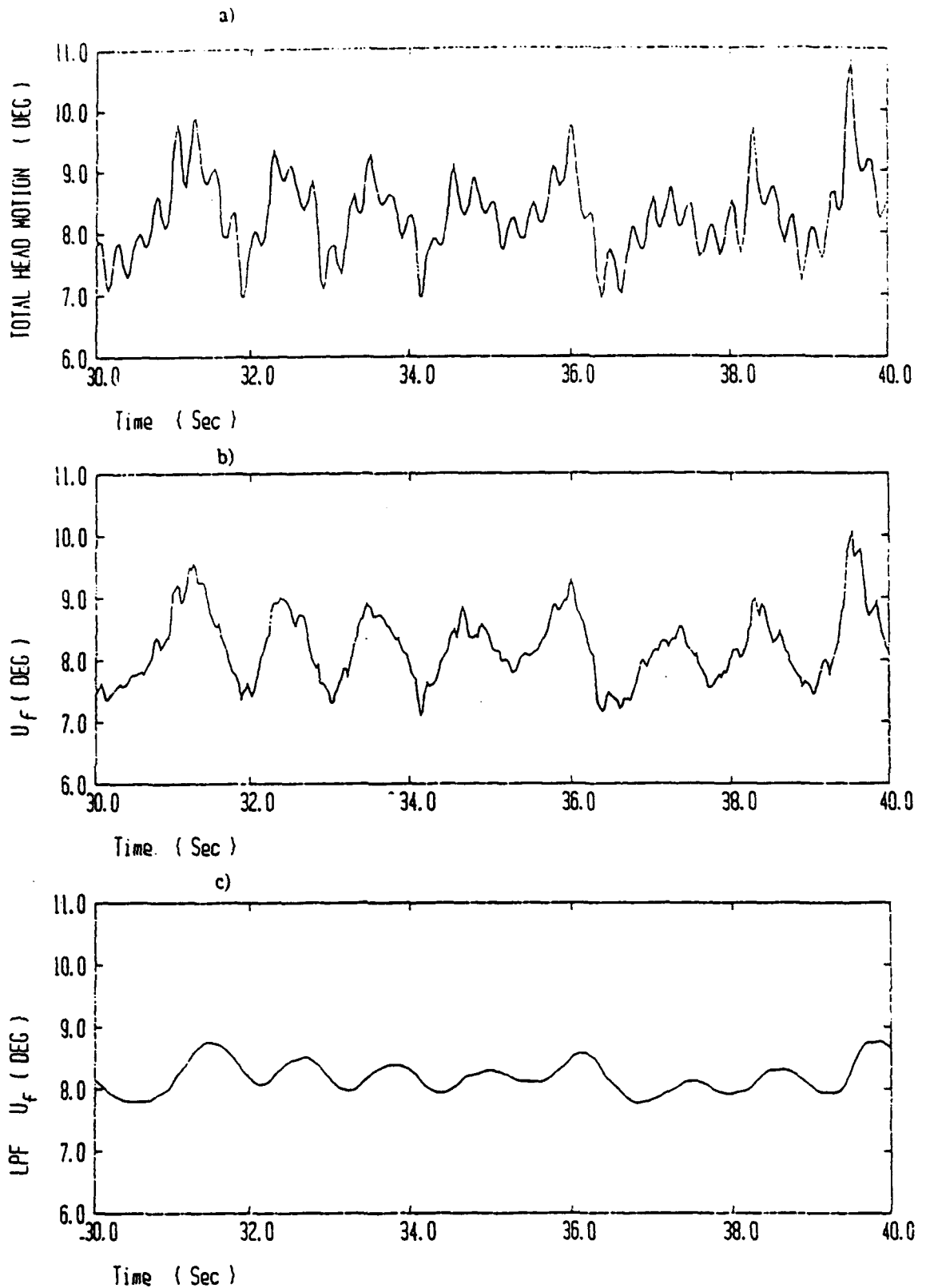


Fig. 7. (a,b,c). A section of the time history of a) total head motion U_t ; b) estimated voluntary head motion U_r ; and c) LPF of U_r , for the example with a moving target (experiment no. 3).

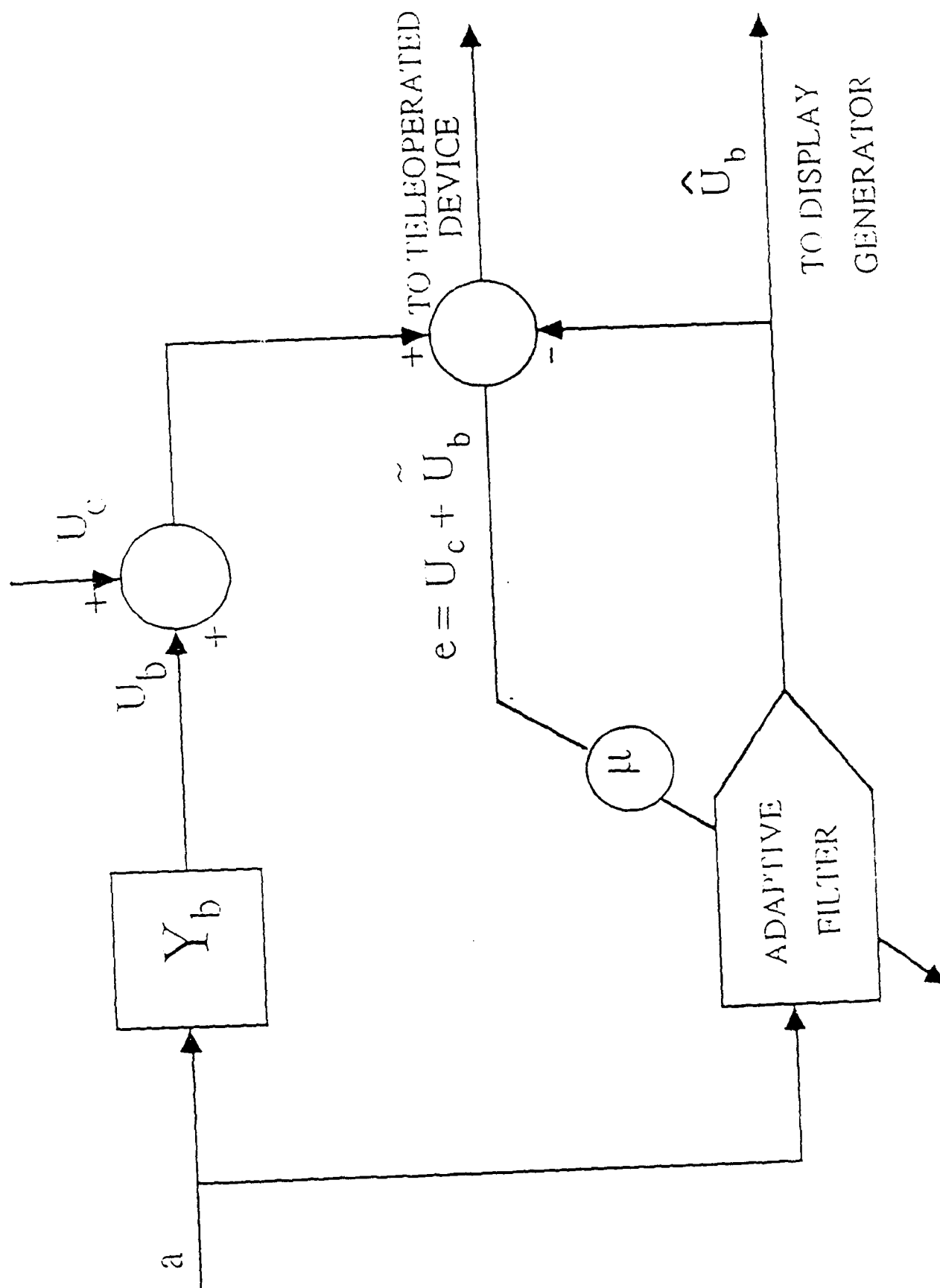


Figure A.1.1. Basic LMS algorithm for suppression of biodynamic interference in HMD and head teleoperation.

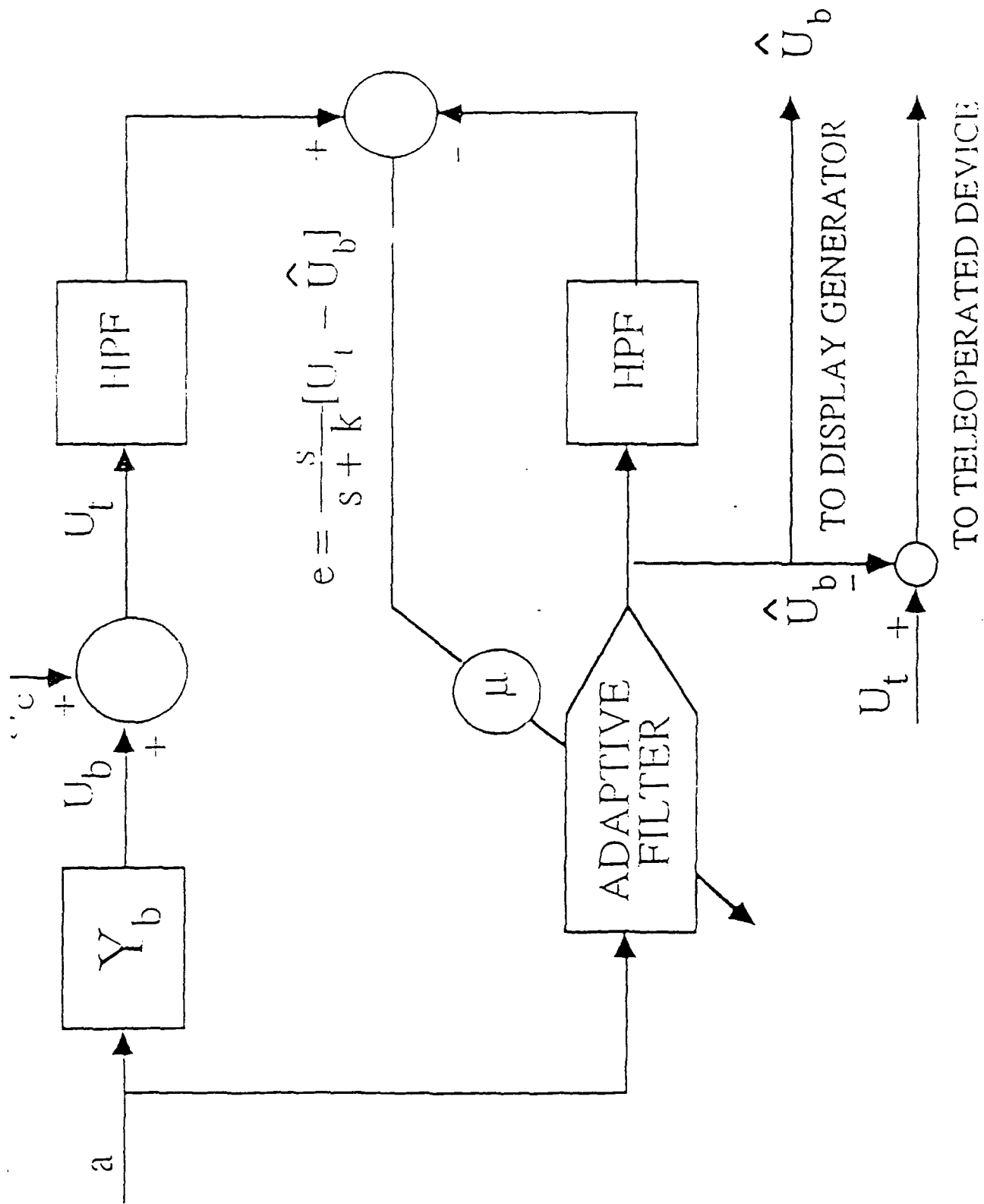


Figure A.2. Extended LMS algorithm for suppression of biodynamic interference in HMD and head teleoperation.